INSTITUTE FOR PHYSICAL RESEARCH AND TECHNOLOGY

IOWA STATE UNIVERSITY
AMES, IOWA 50011

P-36

SPACE LIFE SUPPORT ENGINEERING PROGRAM

ANNUAL PROGRESS REPORT
JULY 1, 1991-JUNE 30, 1992

NASA GRANT NO. NAG 2-722

SUBMITTED TO DR. EDWIN L. FORCE
ADVANCED LIFE SUPPORT DIVISION
NASA-AMES RESEARCH CENTER 239-15
MOFFETT FIELD, CA 94035-1000

PRINCIPAL INVESTIGATOR
DR. RICHARD C. SEAGRAVE
DEPARTMENT OF CHEMICAL ENGINEERING
IOWA STATE UNIVERSITY
AMES, IOWA 50011

PROGRESS REPORT

Space Life Support Engineering Program
Iowa State University
Ames, Iowa

Period: July 1, 1991 through June 30, 1992

Summary

This report covers the first twelve months of work performed under the NASA University Grant awarded to Iowa State University to perform research on two topics relating to the development of closed-loop long-term life support systems.

I. Water Management in Long-Term Closed-Loop Life Support Systems

Overview

A comprehensive study to develop software to simulate the dynamic operation of water reclamation systems in long-term closed-loop life support systems is being carried out as part of an overall program for the design of systems for a moon station or a Mars voyage. This project is being done in parallel with a similar effort in the Department of Chemistry to develop durable accurate low-cost sensors for monitoring of trace chemical and biological species in recycled water supplies. Aspen-Plus software is being used on a group of high-performance work stations to develop the steady state descriptions for a number of existing technologies. Following completion, a dynamic simulation package will be developed for determining the response of such systems to changes in the metabolic needs of the crew and to upsets in system hardware performance.

Personnel: Director: R. C. Seagrave, Distinguished Professor of Chemical Engineering
Post Doctoral Research Fellow: Michael K. Dowd (through October 31, 1991)
Graduate Research Assistant: Dasaratha Sridhar (began October 1, 1991)
Graduate Research Assistant: Sharmista Chatterjee (entire period)
Undergraduate NASA Fellow: Carolyn Pals (through December 15, 1991)
Undergraduate Research Assistants: Amy Weber, Chris Olson

Research Summary

During the first twelve months the following developments have occurred and tasks have been accomplished:

1. Two DEC 2100 workstations and a DEC 3100 color workstation have been configured and supplied with Aspen Plus software. These stations are dedicated to the project.

2. A technical exchange agreement has been executed with Aspen Technology, under which the group at Iowa State and Aspen Plus engineers in Cambridge will exchange visits to assist in the software development for the dynamic modeling programs.

3. Access to the interactive life support system data base at the Ames Research Center has been completed, and it has been made available on all three work-stations.

4. Aspen sub-programs are being developed for the steady-state operation simulation for a closed-loop life support system. The work has been developed as follows:

Water treatment systems: Sharmista Chatterjee (a second year graduate student working on a Ph. D. program)

1. Urine purification
2. Wash water processing
3. Gray water processing
4. Electroincineration of wastes
5. SolidWaste water removal

Air regeneration systems, oxygen generation systems: Carolyn Pals (a last semester senior in chemical engineering and the recipient of a NASA Space Grant consortium summer fellowship and senior scholarship, and Dasaratha Sridhar, (a first-year graduate student in chemical engineering).

1. CO_2 removal
2. CO_2 reduction
3. Oxygen generation
4. Air conditioning
5. Trace contaminant removal

Crew model: Chris Olson (a senior in Aerospace Engineering)

1. Inputs: Height, Weight, Age, Gender, Fitness level, Activity
2. Outputs: Oxygen consumption, CO_2 production, water evaporation, heat production, food consumption, water consumption

Plant Model: Amy Weber (a senior in Chemical Engineering)

1. Inputs: Energy, CO_2, waste products
2. Outputs: Oxygen, water, biomass production

As a basis for beginning, technology designed for Space Station Freedom is being used as the baseline system. Each person is simultaneously investigating alternate technology simulation, and a dynamic model has been developed for the crew. This will be used as a "forcing function" to generate a series of steady-state solutions for the integrated system running under Aspen Plus in a series of interrelated steady states. This baseline set of calculations will serve as the foundation for the dynamic system development.

5. Integration of the individually developed Aspen blocks and Fortran-based models has begun. Dynamic models for the crew members are being developed by modifying an earlier-developed model for predicting the recommended duration of exercise as a function of environmental conditions.

6. The 24 member senior level design class in the chemical engineering department used the long-term closed-loop problem as a senior design class problem, working under the direction of Professors Dean Ulrichson and R. C. Seagrave. This activity has assisted

the group in working through alternate set of scenarios. The design class used a group of 15 DECstation 3100 color workstations for their investigations.

7. In a parallel effort, Seagrave and Chatterjee are performing a thermodynamic analysis (availability analysis) of the closed-loop system in order to identify quantities such as the maximum efficiency, the minimum energy cost, the optimal operating conditions, and the minimum entropy production associated with a life-supported mission. These quantities, expressed as functions of the crew needs and operating parameters such as temperature and pressure, will serve as guideposts in the simulations. Also, this approach should suggest some new criteria for evaluating the relative merits of alternate technologies for the various functions of the system.

8. A dynamic modelling software package (EXTEND, Imagine That, Inc., San Jose, CA) has been obtained and implemented on our machines. It is being used to test preliminary transient models before they are moved to the UNIX-based workstations to make them compatible with the ASPEN-PLUS models. Along with the conversion of the VAX-based dynamic crew model, this now makes a total of three platforms and operating systems that we are integrating, with the goal of reducing this to one flexible system.

9. On October 29, R. C. Seagrave presented a discussion at the Allied-Signal Research Laboratories in Des Plaines, Illinois, on 'Chemical Engineering Problems in Closed-Loop Life Support Systems", and discussed possible collaboration with personnel from the Allied Signal Aerospace Corporation in Torrance, CA.

10. On November 19, R. C. Seagrave visited the group of Dr. P. K. Seshan at the Jet Propulsion Laboratory in Pasadena, CA to discuss aspects of the simulations and future collaboration. One result of this is a modification of the dynamic crew model to include environmental effects on the rate of urine production, which Chris Olson is now implementing.

11. On May 5,6, 1992, Dr. John Finn from NASA Ames Research Center conducted a site visit of the project.

12. On May 12, 1992, Seagrave presented a paper, co-authored with Chatterjee, at the NASA 1992 Life Support Systems Analysis Workshop at the Johnson Space Center entitled "Availability Analysis as a Design Tool for Closed-Loop Life Support Systems". (Copy of transparencies included with this report)

AVAILABILITY ANALYSIS AS A DESIGN TOOL FOR CLOSED-LOOP LIFE SUPPORT SYSTEMS

Sharmista Chatterjee and R. C. Seagrave
Department of Chemical Engineering
Iowa State University
Ames, Iowa 50011

Availability analysis, or exergy analysis, utilizes the first and second laws of thermodynamics to characterize the thermodynamic efficiency of energy conversion systems, or other systems in which entropy is generated in a quantifiable way. Long-term closed-loop life support systems are ideal candidates for such an approach, since the ultimate goal of the designer must be not only to conserve mass and energy, but also to limit the production of entropy to a level compatible with organized life. Living systems require a source of negative entropy, in addition to material and energy requirements. Availability analysis is useful in putting this need in perspective, as well as in evaluating competing technologies for water and air treatment, waste processing, food production, and air conditioning. The closed nature of life support systems allows thermodynamic analysis to proceed more effectively than in many other engineering applications, although the application to such systems is fairly recent.

Presented at the 1992 Life Support Systems Analysis Workshop
Sponsored by the NASA Office of Aeronautics and Space Technology
May 12-14, 1992, Houston, Texas.

MASS BALANCES

Species i

$$\frac{dm_i}{dt} = \sum_{j}^{M} W_{ij} + \sum_{k}^{L} M_i \lambda_{ik} \frac{d\varepsilon_k}{dt}$$

m_i = mass of species i , i = 1, N

W_{ij} = flow rate of species i in stream j , j = 1, M

ε_k = extent of reaction k, k=1, L

λ_{ik} = stoichiometric coefficient of species i in reaction k

Overall-Open System

$$\frac{dm}{dt} = \sum_{i}^{N} \frac{dm_i}{dt} = \sum_{i}^{N} \sum_{j}^{M} W_{ij} + \sum_{i}^{N} \sum_{k}^{L} M_i \lambda_{ik} \frac{d\varepsilon_k}{dt}$$

since this term is zero:

$$\frac{dm}{dt} = \sum_{i}^{N} \frac{dm_i}{dt} = \sum_{i}^{N} \sum_{j}^{M} W_{ij}$$

Overall-Closed System

$$\frac{dm}{dt} = 0$$

ENERGY BALANCES

- negligible mechanical energy effects

Open Systems

$$\frac{dU}{dt} = \dot{Q} + \dot{W} + \sum_{j}^{M} \sum_{i}^{N} H_i \, M_i \, W_{ij}$$

U = internal energy, for which we can also write an "internal relationship" for systems with insignificant volume changes

$$\frac{dU}{dt} = mC_v \frac{dT}{dt} + \sum_{i}^{N} \sum_{k}^{L} H_i \, \lambda_{ik} \frac{d\varepsilon_k}{dt}$$

where this term needs averaged values for the system

and this term represents energy changes resulting from composition changes

Closed Systems

$$mC_v \frac{dT}{dt} + \sum_{i}^{N} \sum_{k}^{L} H_i \, \lambda_{ik} \frac{d\varepsilon_k}{dt} = \dot{Q} + \dot{W}$$

In living systems at a stationary state, between feedings, the second and third terms, both negative, are the dominating terms, with the second term representing metabolic energy conversion, and the third representing the necessary exothermic heat transfer required.

ENTROPY BALANCES

Open Systems

$$\frac{dS}{dt} = \sum_{p} \frac{Q_p}{T_p} + \sum_{j}^{M} \sum_{i}^{N} S_{ij} M_i W_{ij} + \frac{d_i S}{dt}$$

where Q_p and T_p represent the heat flows between the system and the surroundings and the temperatures at which they take place, respectively;

and the last term represents the rate of internal entropy production due to all internal non-equilibrium transport processes, such as heat and mass transfer, fluid flow, and chemical reactions occuring spontaneously;

$$\frac{d_i S}{dt} = \sum_{s} \frac{J_s(-X_s)}{T} \geq 0$$

where the J's and X's represent the flows (fluxes) and driving forces (gradients) respectively.

Closed Systems

$$\frac{dS}{dt} = \sum_{p} \frac{Q_p}{T_p} + \frac{d_i S}{dt}$$

since the last term is always positive, closed systems must rely on the negativity of the heat flow/temperature term to remain at a stationary state. This means they must either operate exothermically.(most living systems) or, if they exist with balanced heat flows in and out,they must take in heat at a higher temperature than they lose it. (the earth)

Living systems have other alternatives...

CLOSED-LOOP LIFE SUPPORT SYSTEMS

The previous considerations now allow us to characterize life support systems from a thermodynamic point of view. Their main functions are:

1. Regulate the m_i's (e.g. oxygen, carbon dioxide, water)

2. Regulate Temperature (one form of U)

3. Provide a source of "negative entropy", and a source of positive free energy.

The implication of (3) is that the LSS must operate in such a fashion so as to mimimize its own entropy production, and to produce low entropy high free energy products from high entropy low free energy wastes.

Availability analysis, or exergy analysis, gives us a method for design the LSS and for evaluating its components so that this goal can be achieved, that is

AVAILABILITY ANALYSIS WILL ALLOW US TO CHARACTERIZE THE LSS AS A NET EXPORTER OF G INTERNALLY AND AS A NET EXPORTER OF S EXTERNALLY.

EXAMPLE OF AVAILABILITY ANALYSIS
(From Bejan, Advanced Engineering Thermodynamics, Wiley, 1988)

Internal Flow and Heat Transfer

Consider the situation in a heat exchanger where we would like to keep the entropy production to a minimum. There are two force-flux entropy producing processes occuring--heat conduction and fluid friction. We would like to determine the appropriate value of the Reynolds number to minimize entropy production.

$$\begin{array}{ccc} & \Delta P & \\ \dot{m} & A & \\ \dot{q} & \Delta T & \end{array}$$

For a length of pipe dx, the energy balance is

$$\dot{m}\, dH = \dot{q}\, dx \qquad \text{where } dH = TdS + VdP$$

The entropy balance is

$$\frac{d_i S}{dt} = \dot{m}\frac{dS}{dx} - \frac{\dot{q}}{T + \Delta T} \geq 0$$

From the definition of internal entropy production

$$\frac{d_i S}{dt} = \frac{q\Delta T}{T^2(1+\Delta T/T)} + \frac{\dot{m}}{\rho T}\left(\frac{-dP}{dx}\right)$$

two flow-force pairs

When we use the appropriate relationships for the friction factor and heat transfer coefficients, this becomes

$$\frac{d_i S}{dt} = \frac{\dot{q}^2}{\pi T^2 k Nu} + \frac{32\dot{m}^3 f}{\pi \rho^2 T D^5}$$

which when solved for the Reynolds number which minimizes this gives

$$Re_o = 2.023\ Pr^{-0.071}\left[\frac{mq\rho}{\mu^{5/2}(kT)^{1/2}}\right]^{0.358}$$

and also results in the two terms in the entropy production relation having the ratio of 6.33.

Now, the ratio of the entropy generated at any given Reynolds number to that at the optimum can be simply derived to produce

$$\frac{\dot{S}_g}{\dot{S}_{min}} = 0.856\left(\frac{Re}{Re_o}\right)^{-0.8} + 0.144\left(\frac{Re}{Re_o}\right)^{4.8}$$

which has the following interesting shape:

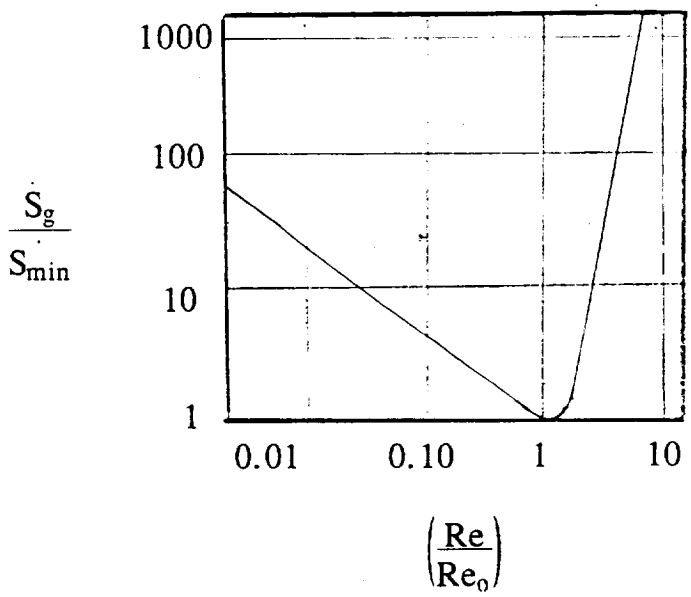

MASS EXCHANGERS

For components which exchange mass (e.g. separators, reactors, absorbers) the entropy production term can be written in general as:

$$\frac{d_i S}{dt} = -\frac{1}{T}\sum_{i}^{N} j_i \nabla\mu_i + \frac{\mu}{T}\phi - \frac{1}{T^2} q.\nabla T - \frac{1}{T}\sum_{i}^{N} S_i j_i \nabla T$$

where the first term on the left accounts for mass fluxes driven by chemical potential differences, the second, viscous dissipation from fluid friction, the third, heat fluxes resulting from temperature gradients, and the fourth coupling between heat and mass transfer.

APPROACH

The approach is now two-fold:

1. Examine a proposed CELSS by quantifying its overall efficiency as an entropy producer and as a supplier of free energy. This notion can allow comparison of different configurations, and provides another design criteria useful in a larger sense. Also, it can help to determine the nature of an "ideal" CELSS, which, like any closed system, is subject to thermodynamic limitations.

2. Perform availability analysis on existing technologies proposed for inclusion in manned space flights, such as VCD, TIMES, 4BMS, and so on, to gain new insight on their overall contribution to the life support mission.

NASA Sensor Program Progress Report
M. Porter

Overview. This program focuses on designing and testing novel sensor technologies for operation in long-term closed-loop life support systems. Such applications present a unique set of challenges with respect to size, durability, reliability, and, in particular, detection specificity and sensitivity. To meet these needs, approaches to manipulate the molecular architecture of various transducer surfaces (e.g. bulk and surface acoustic wave resonators, optical fibers, and electrodes) are being developed. Efforts to devise enabling strategies for implementation of the noted transducer technologies are also underway.

Personnel.

Dr. Marc D.Porter	Assistant Professor of Chemistry and MicroAnalytical Instrumentation Center
Dr. Glenn J. Bastiaans	Acting Director, MicroAnalytical Instrumentation Center
Dr. Stanley G. Burns	Professor of Electrical Engineering
Dr. Duane E. Weisshaar	Visiting Scientist
Dr. Mary M. Walczak	Institute for Physical Research and Technology Post-Doctoral Fellow
Mr. Ronald P. O'Toole	Graduate Research Associate

Research Summary. Efforts in the past six months have focused primarily on three general areas: (I) the evaluation of the performance characteristics of a new type of piezoelectric mass sensor; (II) the initiation of an exploration of coating chemistries for the development of detection specificity; and (III) the development and testing of a protocol for location-specific coating deposition.

(I). Performance Characteristics of a High Sensitivity Mass Sensor. This portion of our effort focused on the testing of a new form a piezoelectric mass sensor. The sensor has a high mass sensitivity (minimal detectable mass of ~2 ng/cm^2), is small in size, and can potentially be mass produced at low cost. The sensor is a thin film bulk acoustic wave resonator, which consists of an oriented aluminum nitride membrane situated between two metal electrodes. The sensor is fabricated by sputtering aluminum in a low pressure N_2 atmosphere onto a silicon substrate. This process forms a thin film of piezoelectric aluminum nitride. After etching the silicon from beneath the aluminum nitride layer, gold electrodes were patterned on both sides of the resulting membrane to complete fabrication. This procedure produces a thin (5.5 μm) film resonator (TFR) that is shaped as a 400 μm square and supports a standing bulk acoustic wave (logitudinal mode) at frequencies of ~1 GHz. Such small sizes open the possibility of integrating as many as 200 TFRs, each conceivably configured for the detection a specific analyte, onto a single 76 mm diameter silicon wafer. In addition, the high resonance frequencies translate to detection sensitivities that rival those of the most sensitive mass sensors currently available, but in a much smaller device package. A schematic drawing of a TFR is shown in Figure 1. Table I presents the results of the sensitivity tests, comparable data for other types of mass sensors, and a brief description of the experimental protocol of these tests.

Since completion of these tests, we have cut, mounted, and wire bonded our TFRs onto standard intergrated circuit carriers. These carriers (volume: < 10 mL) have been modified to accept analyte gases, with the completed package facilitating performance testing (e.g. specificity of interactions between a coating and gas phase analyte) as well as

interchange of samples. A fixtured TFR in a carrier is shown in Figures 2 and 3. A gas blending and flow system is nearing completion, along with software for automated instrument control of both the flow system and vector voltmeter.

(II). Preliminary Testing of Possible Coating Chemistries. An example of recent results from this phase of the program are given in both Figure 4 and Table II. These experiments employed TFRs that were coated with a monolayer of a fluorinated ($CF_3(CF_2)_7(CH_2)_2S$) and a carboxylic acid-terminated ($HOOC(CH_2)_{15}$)S thiolate adsorbed at the topside gold electrodes on a TFR. These experiments were designed to demonstrate the mass detection capability of the TFRs, to assess the utility of the adsorption of thiol compounds for selective coating preparation, and to begin to collect a set of fundamental data to aid the predictive design of coating with specific sorption characteristics. The fluorinated monolayer has an extremely low critical surface tension (5-10 mN/m), and, as such, should display little affinity for adsorption of a test gas such as methanol. Conversely, a carboxylic acid-terminated monolayer presents a more reactive functional group at the air-monolayer interface. The latter films are wetted by methanol, a consequence of both the polarity and hydrogen-bonding interactions of the end group. The results of these tests (Figure 4 and Table II) are consistent with the predicted behavior. That is, the relative change in the resonance frequency ($\Delta F_s/F_s$) of the TFR coated with the carboxylic acid-terminated monolayer is much larger than that of the CF_3-terminated monolayer. Additionally, the responses return to their initial values upon purging methanol from the test chamber. This indicates the sorption of methanol at both surfaces is reversible. It is also important to note that the responses are nonlinear with methanol concentration. This reflects saturation of the surface with the adsorbate. The response of the carboxylic acid-terminated monolayer with the 0.4 mL methanol injection corresponds to a mass increase of 29 ng/cm^2 (i.e. an absolute mass of ~40 pg), which is close to that expected for a 1:1 binding stoichiometry between methanol and the end group. Efforts along these lines are continuing, with preliminary tests of amine-terminated monolayers for CO_2 detection.

(III). Preliminary Testing of a Location-Specific Deposition Procedure. In a companion effort, we have begun to devise approaches for the "location specific" deposition of our thiolate monolayers at gold ($X(CH_2)_nS$-(Au(1)), X= $-CH_3$, -OH, CF_3, - NH_2). The goal is to modify selectively a specific site on a microfabricated sensor array. In the case of our TFRs, this effectively translates to the deposition of a thiolate monolayer of a specific composition on one membrane without perturbing that on a neighboring membrane. Such a requirement demands a high level of control over the spatial resolution of the deposition process since separation distances between neighboring TFRs may only be a few microns. We have addressed this issue by taking advantage of our recent discovery that thiolate monolayers can be deposited by a one-electron oxidative deposition process in alkaline (pH > 11) solution: RS^- + Au(0) --> RS-(Au(I)), a finding that derives from our earlier studies of the reaction involved in the formation of these monolayer from the corresponding thiol. To test this approach, we prepared a set of interdigitated gold bands. These bands were patterned by standard microlithography techniques. Each band is 3 μm in width with a 3 μm separation distance between bands. Preliminary tests were conducted using scanning Auger spectrometry to detect and map the location of a CF_3-terminated monolayer. The CF_3-terminated monolayer was selected in this first study because of the high sensitivity of Auger spectrometry for fluorine. Results show that Auger spectroscopy has both the resolution and sensitivity detect the presence of CF_3- as well as $-NH_2$ and ferrocenyl-terminated monolayers. We next plan to determine if deposition can be confined only to those bands held at an applied potential that leads to film formation.

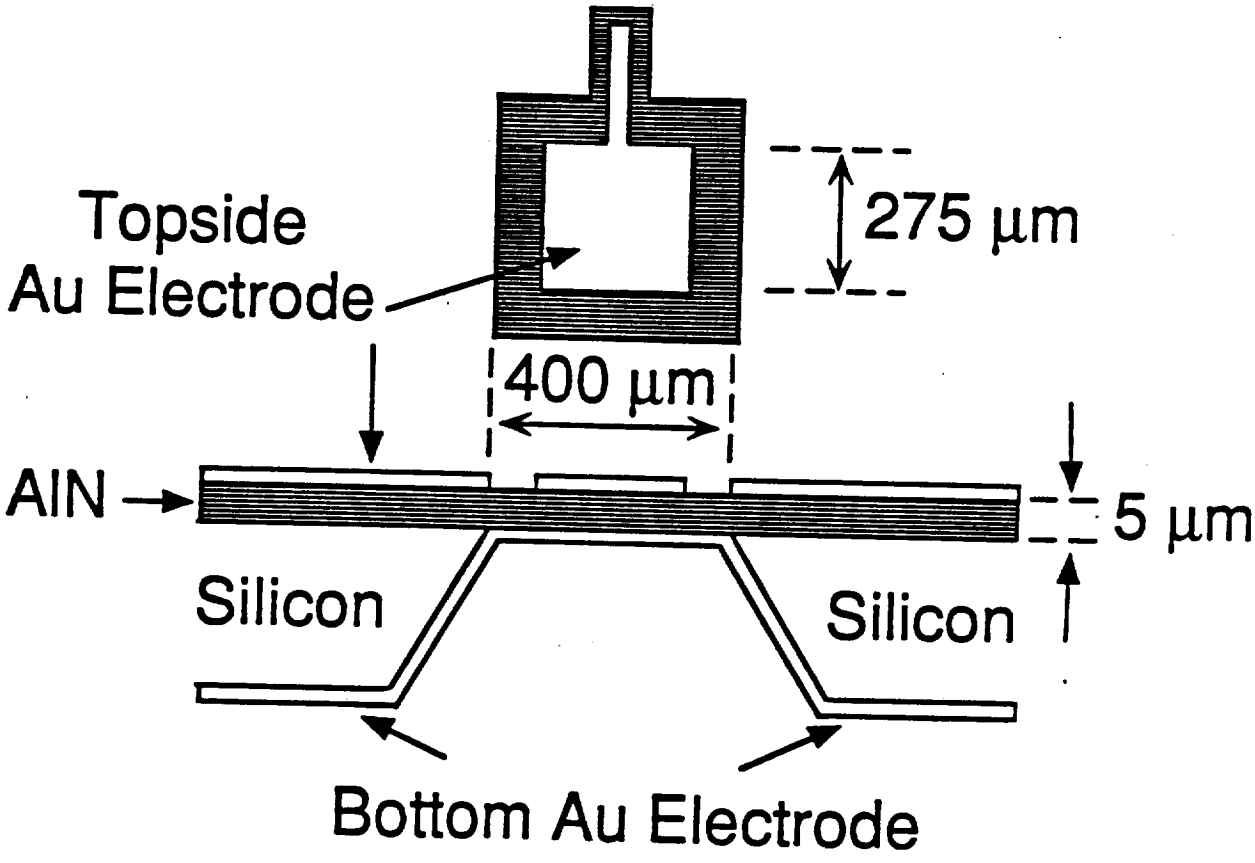

Figure 1. Schematic diagrams of a TFR. The upper portion is a top view where the Au electrode is shown in white and the underlying aluminum nitride membrane is shown by the hatch- markings. The lower portion is a side view which illustrates the layer structure of the composite material.

Novel Approaches to the Construction of Miniaturized Analytical Instrumentation

Marc D. Porter	Iowa State University
Ronald P. O'Toole	Iowa State University
Shelley J. Coldiron	Iowa State University
William D. Deninger	Iowa State University
Randall S. Deinhammer	Iowa State University
Stanley G. Burns	Iowa State University
Glenn J. Bastiaans	Iowa State University
Steve D. Braymen	Iowa State University
Howard R. Shanks	Iowa State University

ABSTRACT

This paper focuses on the design, construction, preliminary testing, and potential applications of three forms of miniaturized analytical instrumentation. The first is an optical fiber instrument for monitoring pH and other cations in aqueous solutions. The instrument couples chemically selective indicators that have been immobilized at porous polymeric films with a hardware package that provides the excitation light source, required optical components, and detection and data processing hardware.

The second is a new form of a piezoelectric mass sensor. The sensor was fabricated by the deposition of a thin (5.5 μm) film of piezoelectric aluminum nitride (AlN). The completed deposition process yields a thin film resonator (TFR) that is shaped as a 400 μm square and supports a standing bulk acoustic wave in a longitudinal mode at frequencies of ~1 GHz. Various deposition and vapor sorption studies indicate that the mass sensitivity of the TFRs rival those of the most sensitive mass sensors currently available, though offering such performance in a markedly smaller device.

The third couples a novel form of liquid chromatography with microlithographic miniaturization techniques. The status of the miniaturization effort, the goal of which is to achieve chip-scale separations, is briefly discussed.

INTRODUCTION

Interest in the design, development, and application of chemical sensors has grown explosively in the past several years (1-3). The impetus for this growth derives from the increasing technological need to perform analytical measurements remote from a central laboratory and in a variety of complex settings. Environmental monitoring and process control serve as examples of such needs. There is a general consensus that such sensors be small-sized, durable, have responses specific to a given analyte or classes of analytes, and be fabricated at low cost. The latter attribute enhances deployment in large numbers or as devices with limited operational lifetimes.

More specific attributes are largely application dependent. In a monitoring application, for example, the response of a sensor may need to be reversible. An irreversible response, however, may facilitate usage for dosimetry purposes. Some applications may require large scale deployment, with sensors located at a large number of sampling sites. Detecting and following contaminant plume migration in an aquifer serves as an example. In such a mode, periodic interrogation of the collected data via a telemetric data link would be preferable. In contrast, the operational machinery and piping in an industrial plant may interfere with a telemetric system, dictating the usage of direct hardwire data links.

The development of durable miniaturized analytical instrumentation for chemical sensing is also critical for meeting the many challenges of life-support in the space program. Issues such as small payloads and operation over a wide range of temperature and pressure are requisite for space exploration and colonization. Specific applications, such as space water management, demand the integration of chemically specific sensors with feedback control systems for continuous process monitoring and adjustment of purification systems. Not only must the sensor hardware exhibit both chemical specificity and sensitivity, it must be integrated "on-line" with the processing system to provide the requisite feedback for system adjustment. Thus, meeting the challenges for the development of sensors with specific performance characteristics will require an increasingly interdisciplinary research strategy, drawing from such fields as synthetic organic chemistry, interfacial chemistry, materials science, and computer and electrical engineering.

This paper presents a progress report of the ongoing sensor development efforts at the Analytical Instrumentation Center at Iowa State University. The status of three related projects are presented, each of which are at various developmental stages. The first two sections also addresses issues related to the interfacial chemistry of the sensors, and how to manipulate coatings to achieve the targeted selectivity.

The first project involves the construction and performance characterization of a small-sized fiber optic spectrometer for solution-phase analysis (4). As presently configured, the instrument functions in an absorbance mode as a solid-state, dual-beam spectrometer and is equipped with a custom-designed controller, data processor, and telemetric communications hardware.

The second project focuses on the development of a new form of piezoelectric mass sensor (5). Such sensors exhibit a response at low loading levels that is proportional to the mass of a sorbed analyte. The sensor is based on thin film resonator (TFR) technology, consisting of a thin (5.5 μm) oriented aluminum nitride membrane located between two metal electrodes. The sensor, created by coating the TFR surface with a self-assembled monolayer to demonstrate a primitive form of analyte selectivity, exhibits mass sensitivities that rival those of the most sensitive mass sensors currently available, while offering such performance in an extremely small-sized package (400 μm squares).

The third project involves a departure from the general strategies of the first two, focusing on the design, development, and testing of a miniaturized novel (6) form of ion chromatography. The goal of this project is the integration of the components of conventional liquid chromatography to chip-scale sizes. Such a development would provide a separation step prior to detection via various sensor transduction schemes. The status of this project is updated.

DUAL-WAVELENGTH FIBER OPTIC SENSOR INSTRUMENTATION

One of the many challenges of space exploration is the development of compact, durable and reliable instrumentation for incorporation into a life support system. The focus of this project is on the development of fiber optic sensor instrumentation for monitoring the physiological status of astronauts during extended missions. Conventional analytical instrumentation, however, only partially fulfills these needs. For example, common procedures for direct analysis of important electrolytes and minerals (e.g. sodium, potassium, and calcium) employ flames, plasmas or electrical arcs for sample atomization and excitation, facilitating assay of the target analyte by emission or absorbance (7). These instruments are large and require expendable support materials, i.e. fuel and oxidant gases for flames and plasmas. Since the exploration of space and colonization of extraterrestrial bodies places extreme limitations on payload size, the expansiveness of conventional analytical instrumentation dictates development of novel, miniaturized instrumentation.

Figure 1 depicts the major components of the fiber optic sensor, illustrating its attributes. The attributes derive from the combination of three diverse research areas: fiber optic technology, organic thin-film surface chemistry, and electronic hardware design. The union of these three research areas facilitates the conception, design, and application of integrated, sensitive chemical sensors and hardware processing and telemetry systems.

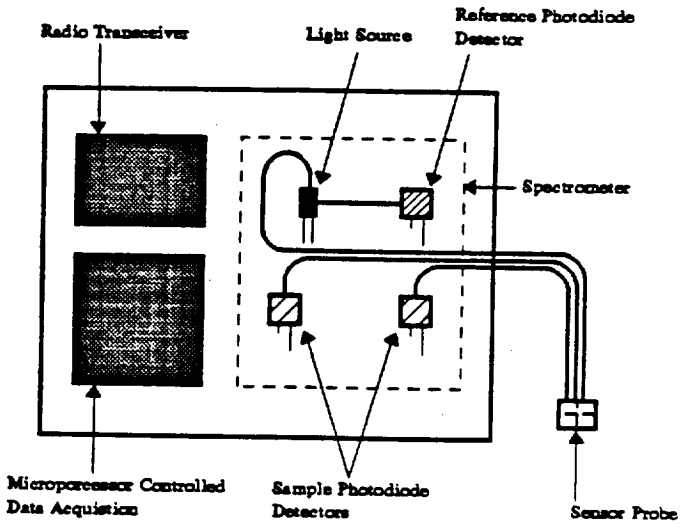

Figure 1. Miniaturized Optical Sensor Instrument.

THIN FILM SENSOR DEVELOPMENT - The development of reversible multicomponent optical electrolyte sensors that can be used for whole blood measurements remains a significant challenge. Current optical pH sensor technology is hampered by the inaccuracies resulting from variations in blood ionic strength (8). Also, since most of the sensor materials are constructed from an impermeable thin film of an organic polymer, response times can be as long as 10 minutes, which limit overall utility.

In earlier work, we first addressed these issues though the development of a highly selective pH sensor (pH range 0-4.5) with a response time of less than 2 sec (9). The sensor was constructed by immobilizing Congo Red at a base-hydrolyzed cellulose acetate film. The rapid response results from the porous structure of the hydrolyzed polymeric support, which reduces barriers to mass transport between the analyte and immobilized indicator. A generalization of the preparative route is shown in Figure 2 and can be readily coupled to other immobilization schemes.

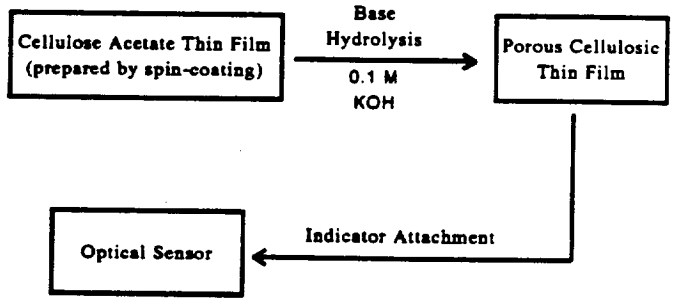

Figure 2. Indicator Immobilization at Porous Cellulosic Films.

Different indicators have been tested for application at physiological pH. Brilliant Yellow, which has an optical transition in solution between pH 6 and 8, was one of the first indicators investigated. However, upon immobilization, the optical transition occurs at higher pH values (i.e. ~2 pH units), an effect frequently observed as a consequence of immobilization (10). Of the many indicators surveyed, fluoresceinamine demonstrated the desired optical transition for detection of physiological pH with immobilization.

Initial indicator attachment techniques with Congo Red utilized non-covalent adsorption of the dye with the cellulosic film (9). However, to increase the long-term stability of the sensor, covalent bonding of the indicator with the film is preferable. Several established linkage techniques were tested such as coupling through cyanuric chloride (11) and cross-linking with glutaraldehyde (12). However, once immobilized, most of the indicators investigated lost their chromophoric transition properties.

The use of polymer beads for coupling and immobilization of indicators is under investigation. Riedel-deHaën produces a polymer carrier for the covalent immobilization of enzymes, Polymer Carrier VA-Epoxy BIOSYNTH®. Chemically, it is a copolymer based on vinyl acetate and divinylethylene-urea whose surface is modified with oxirane groups after hydrolysis of the acetate groups. These epoxide linkages can be utilized to couple various compounds as depicted in Figure 3.

Acid-catalyzed linkage with hydroxyl groups.

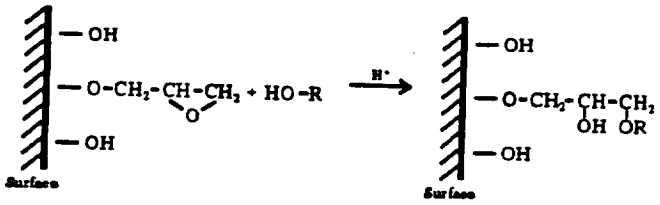

Base-catalyzed linkage with amine groups.

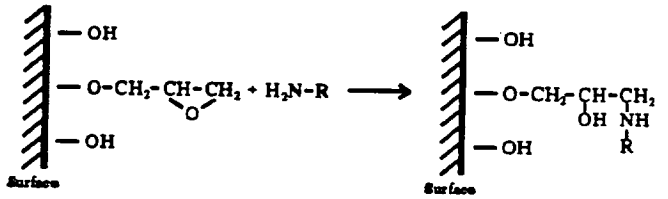

Figure 3. Acid and Base Reactions of Epoxide Linkages.

Fluoresceinamine was coupled to the epoxy beads by weighing 1:1 indicator to bead weight followed by immersion in 1 M Na_2HPO_4. The suspension was stirred for 48 h and excess dye was removed by washing the beads with 0.1 M Na_2HPO_4. The dried product was suspended in a 14% w/w cellulose acetate/cyclohexanone solution. The suspension was sonicated to disperse the beads within the viscous solution. The cellulosic suspension was cast by spin coating onto a glass slide and dried at 70°C for ~12 h. The dried films were then hydrolyzed with 0.1 M KOH for 24 h.

The beads lend strength to the cellulosic films and are easily handled. Without the beads, the films are mechanically weak. The films exhibit both visible and fluorescent spectroscopic transitions with changes in pH from 3 to 9. The indicator behaves as a polyprotic acid with absorption maxima at 440 nm, 460 nm, and 500 nm, which will facilitate the development of an internally calibrated sensor by calculating the ratio of the absorption maxima for each form of the indicator. Such an approach also compensates for calibration difficulties that may arise from preparative variations in the amount of immobilized indicator and the desorption loss of the indicator from the film during use.

INSTRUMENT DEVELOPMENT - Photometer Design - A schematic diagram of the photometer is shown in Figure 4. White light from a miniature lamp is carried to the sensor probe by a single-stranded optical fiber. Another fiber carries a portion of the light from the lamp to a reference detector. Two single-stranded fibers collect and transmit light from the sensor probe to the sample detectors. This design represents a variation from the original prototype which used light emitting diodes as light sources and several other optical components (4). The revised prototype enhances light throughput and utilizes electrical components with greater sensitivity and stability, thereby improving overall instrument sensitivity.

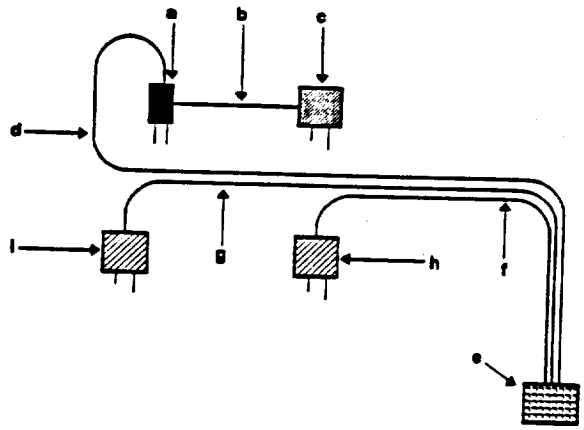

Figure 4. Photometer Schematic. a) White Light Source; b) Single Fiber to Reference Detector; c) Reference Detector; d) Single Fiber to Sensor Probe; e) Sensor Probe; f & g) Fibers to Signal Detectors; h & i) Signal Detectors with Interference Filters.

The light source is a miniature, gas-filled tungsten lamp from Carley Lamps (#T 1 1/2, 631L). The greybody radiator emits over the visible spectral range. An end lens on the lamp minimizes energy loss from refraction. Additionally, the lamp is positioned within an elliptical reflector (Carley Lamps, #1580) to focus and collimate energy that would be lost through spherical radiation. As described in our earlier work, the collimated beam is focused by a graded refractive

index lens (GRIN) onto the tip of the optical fiber that illuminates the sensor probe (4).

The detector housings (see Figure 5) contain silicon photodiodes (EG&G VACTEC, VTB 9414) with active areas of 1.6 mm^2. The sample detectors measure the light intensity after passing through the sensor probe. The reference detector measures the intensity of the light directly from the lamp. Light from the optical fibers are coupled to interference filters. The selected spectral band is focused upon the detectors with GRIN lenses. The photodiodes are enhanced in the UV to IR spectral range with low dark currents and very high shunt resistances to provide a very low offset in high gain transimpedance connected operational amplifier circuits.

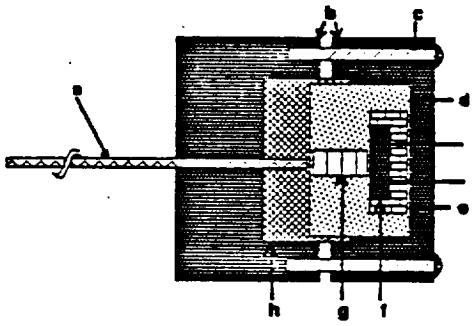

Figure 5. Detector Housing Assembly. a) Single Fiber; b) PVC Assembly Body Housing; c) Nylon Screws; d) Delrin Filter Adapter; e) Delrin Detector Housing; f) Photodiode; g) GRIN Lens; h) Interference Filter.

The photodiodes are connected in a photovoltaic mode to transimpedance operational amplifiers (AD549, Analog Devices). The amplifiers have a common-mode impedance of 10^{15} ohms with an extremely low bias current of 250 fA maximum. The operational amplifier performs well as a sensitive photodiode preamplifier because of its low input current and offset voltage characteristics. Gain is achieved with use of feedback resistance.

The optical fibers have a 400 μm silica core diameter, which is coated by a 80 μm thick fluorine doped silica cladding (UV400/480N, Ceramoptec). The ends of the fibers are polished to a mirror like finish prior to connection with successive grades (32, 15, 3, and 0.3 μm) of abrasive sheets. The all silica construction of the fibers enhances spectral transmission from the UV to IR spectral range over standard communication optical fibers.

Sensor Probe Design - A diagram of the sensor probe is shown in Figure 6. The probe body is constructed from two Delrin discs (1.6 cm diameter and 0.64 cm thick). The top plate serves as a mount for both the input and the collection fibers. The bottom plate houses a GRIN lens. The distal surface of the GRIN lens is coated with a reflective silver film (800 nm thick), which is protected from solution by a coating of epoxy cement. A Nylon plate (0.1 cm thick) is used to mount the thin-film sensor firmly on top of the GRIN lens; a 0.15 cm diameter hole is drilled through the plate to expose a portion of the sensing film to solution and to the incident light beam. Nylon guide pins facilitate optical alignment of the fibers with the GRIN lens and control the separation distance between the Delrin plates. The spacing between the fibers and the thin sensing film (~0.5 cm) provides a clear path for solution to flow over the sensing element. Fully assembled, the probe is 1.7 cm in length and 1.6 cm in diameter.

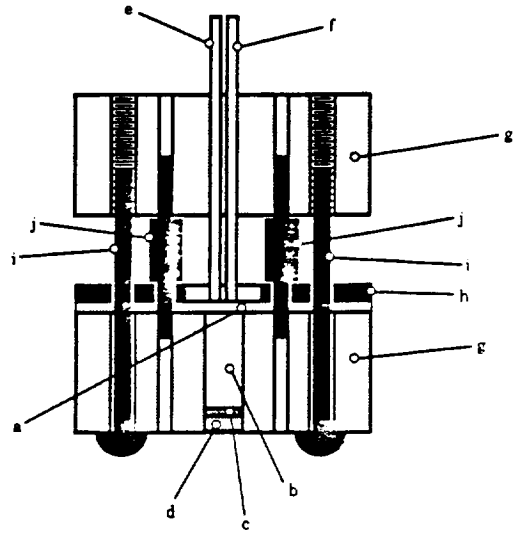

Figure 6. Fiber Optic Sensor Probe. a) Sensing Film; b) GRIN lens; c) Silver Film Mirror; d) Epoxy Cement; e) Input Fiber; f) Collection Fibers; g) Probe Body; h) Retainment Plate; i) Locking Screws; j) Guide Pins.

The GRIN lens steers light from the input fiber of the sensor probe to the collection fibers. To maximize light coupling, the fibers are spaced at an equal distance radially around the lens. The mirrored back surface of the lens serves to reflect the incident radiation. It is important to note that the sampling beam makes two passes through the sensing film prior to transmission back to the photometer.

ADVANTAGES AND ADDITIONAL APPLICATIONS - Advantages - The conceptual basis of these sensors offers several major technological advantages in addition to those described. First, the use of fiber optic sensors facilitates miniaturization of instrumentation. These devices could conceivably be modified and reduced in size for implantation thereby facilitating continuous monitoring of physiological parameters. Miller demonstrated short term biocompatibility of fiber optic sensors for implantation in dogs during a 4 hour catheterized femoral artery study by coating the fibers with a layer containing covalently bonded heparin to prevent thrombosis (13).

Secondly, electrical isolation of these proposed devices provide an added safety feature by prevention of electrical shock. A major concern of invasive devices (e.g. catheters) is inducement of microshock. When the epidermal layer is violated, small currents (on the order of microamps) conducting across heart muscle can lead to fibrillation (14). Fibrillation, unless intervened by defibrillation procedures, can lead to a 'heart attack' and death (14).

Additional Applications - The sensor device described within this paper could be modified for detection of other

analytes. In the sustainable biosphere of a space station or lunar colony, air and water will need to be continuously repurified and recirculated, demanding reliable methods for monitoring removal of toxic wastes and contaminants (15).

As configured, the instrument contains no mechanical components and operates in a fixed-wavelength mode, while maintaining the precision and accuracy of earlier reported fluorescence-based laboratory measurements (16). Based upon construction with low-cost components, small size, mechanical durability, and minimal need for calibration, the instrument would be aptly suited for field deployment in environmental applications. The device could serve as a prototype for development of sensors to detect environmental analytes. Conceivably, modifications would entail: identification and immobilization of proper indicator compounds, replacement of optical filters for different spectral response ranges, and encasement of the hardware package for operation in hostile locations.

Efforts to construct "remote sensing modules" (RSMs) that will use the photometer as the central component are nearing completion. The RSMs, will contain on-board microprocessors for instrument control and FM-radio transceivers for data transmission to a centralized computer system. The microprocessors will control photometer operation and the transceivers will provide wireless data communications.

THIN FILM RESONATORS : A NEW FORM OF PIEZOELECTRIC MASS SENSORS

Piezoelectric mass sensors are solid state devices that respond to changes in temperature, pressure, and most importantly, the physical properties of its interface. Such changes include interfacial mass density, elasticity, viscosity, and sorbed layer thickness. The sensors operate by monitoring the propagation of an acoustic wave through the solid state device. A most common mass sensor is an acoustic bulk wave resonator which is constructed by depositing metal electrodes onto a thin piezoelectric material.

This section briefly summarizes the results of feasibility studies which have established currently achievable mass sensitivities and demonstrated the potential of TFRs as the transducer component in a gas phase chemical sensor. The sensor is based on thin film resonator technology (5, 17-20), consisting of an oriented aluminum nitride membrane situated between two metal electrodes. The sensor has a high mass sensitivity, (S_m, ~550 cm^2/g), is small in size, is easily fabricated, and can potentially be mass-produced at low cost. Using microlithographic techniques, gold-coated TFRs were produced as 400 μm squares with a 5.5 μm membrane thickness (Figure 7). Such small sizes open the possibility of integrating as many as 200 TFRs and associated support electronics onto a single 76 mm diameter silicon wafer. The membrane thickness lead to resonance frequencies of ~1 GHz. As will be demonstrated, these high resonance frequencies translate to mass sensitivities that rival those of the most sensitive mass sensors currently available, while offering such performance in an extremely small-sized package.

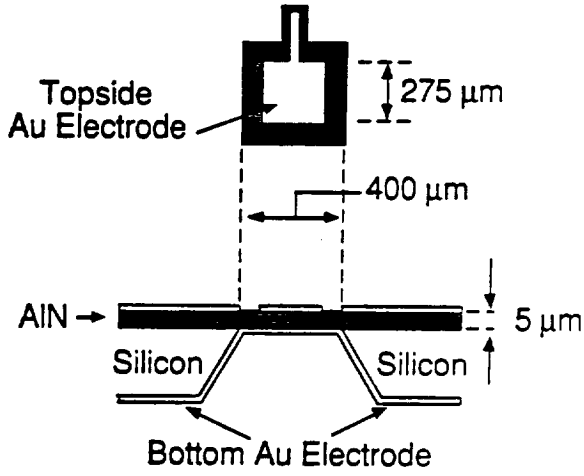

Figure 7. Schematic diagrams of a thin film resonator. The upper portion is a top view where the Au electrode is shown in white and the underlying AlN membrane is shown by the hatch-markings. The lower portion is a side view which illustrates the layered structure of the composite material. See references 5, 17-20 for preparation details.

Sauerbrey first demonstrated that acoustic bulk wave resonators could be used as mass sensors (21). As shown by the classic Sauerbrey equation (Eqn. 1), the relative change in series resonance frequency is linearly related to the mass of a material sorbed on a resonator surface (21, 22), $F°_s$ is the initial series resonance frequency, ΔF_s is the change in series resonance frequency after the deposition of the material, ΔM represents the change in mass per unit surface area arising from analyte sorption, ρ_s is the density of the resonator material, and C_s is the stiffness constant of the membrane. A negative sign on the right hand side of Equation 1 therefore indicates that F_s decreases with increases in sorbed mass. It is important to note that Equation 1 is accurate only for mass depositions less than 2% of the mass of the resonator (22-24) and neglects any effects of differences in the elasticity and/or viscosity of the sorbed material with respect to the resonator material (25-28).

$$\frac{\Delta F_s}{F_s^\circ} = \frac{-2F_s^\circ \Delta M}{[\rho_s C_s]^{1/2}} \qquad (1)$$

The mass sensitivity, S_m, of a bulk acoustic wave resonator is defined, following Wenzel and White (29), as

$$S_m = -\frac{2nF_s^\circ}{\rho_s V} \qquad (2)$$

where n is an integer designating the resonance mode and V is the velocity of the acoustic wave. Since S_m is inversely proportional to resonator thickness, the AlN TFRs are

predicted to have an extremely high mass sensitivity (see Table I).

Table I. Performance Characteristics of Various Piezoelectric Mass Sensors.

Device	Operating Frequency (MHz)	Calculated S_m(cm^2/g)	Experimental S_m(cm^2/g)
QCM[a]	6	-14	-14[d]
SAW[b]	112	-151	-91[e]
	200	-252	-263[f]
	400	-505	-493[f]
FP[c]	2.6	-951	-990[g]
TFR	965	-567	-509[h,i]
	982	-574	-555[j]

a) Quartz Crystal Microbalance. b) Surface Acoustic Wave. c) Flexural Plate. d) Reference 23. e) Reference 39. f) Reference 40. g) Reference 29. h) See reference 5 for a description of measurement protocols. i) PMMA loading experiments (film thickness of 21.7 $\pm$ 0.7 nm). j) Monolayer loading experiments (based on the difference in F_s for films formed by the spontaneous adsorption of $CH_3(CH_2)_3SH$ and $CH_3(CH_2)_{17}SH$).

MASS SENSITIVITY (S_m) TESTS - The sensitivity of the TFRs to mass loading was determined by two different experiments, the results of which are summarized in Table I. The first experiment monitored the effect of the deposition of a 21.7 $\pm$ 0.7 nm film of PMMA on the resonator properties. Measurements were taken on several TFRs with typical absolute and relative frequency changes after coating of 35 kHz and 39 ppm, respectively. Based on the coating thickness and the density of bulk PMMA (1.2 g/cm^3) (30), ΔM was calculated.

In the second experiment, the TFR response was first measured after adsorption of a monolayer formed from butanethiol ($CH_3(CH_2)_3SH$). The TFRs were next cleaned and coated with a monolayer from octadecanethiol ($CH_3(CH_2)_{17}SH$). The TFR responses were again measured. Since both monolayers form structures with comparable surface coverages (9.1 $\pm$ 0.5 x 10^{-10} moles/cm^2 (31, 32)), the difference in mass loading between the two monolayers was calculated from their chain length differences. Such tests using uncoated TFRs were hindered because of contaminant adsorption at the "bare" gold surface.

From the results of the two different mass loading experiments, experimental values of S_m were calculated. Equation 2 was used to compute a S_m based on F_s and literature values of ρ_s and V (33). Table I summarizes the results and provides comparison data for other forms of piezoelectric mass sensors. As is evident, the average experimentally determined values of S_m (-509 and -555 cm^2/g) are comparable to those predicted by theory (-567 and -574 cm^2/g), consistent with the performance expected for a well-behaved mass sensor. More importantly, these results show that the TFRs exhibit a much greater intrinsic sensitivity to mass loading than the QCMs. Only the flexural plate and the high frequency (i.e., 400 MHz) SAW devices, which are both markedly larger in size and have much more complex electrode patterns, have comparable sensitivities.

DEMONSTRATION OF PERFORMANCE OF TFRs AS A GAS PHASE SENSOR - As is the case for many types of chemical sensors, the performance of piezoelectric mass sensors is as much or more a function of the surface coating as it is of the mass response characteristics. The properties of the coating determine the rate of the response, reversibility, and selectivity. The coatings also play a major role in defining the relationship between analyte concentration and analytical response. Therefore, the choice of the coating is one of the most critical aspects of sensor design. To demonstrate the feasibility of using TFRs as sensors, two relatively simple sets of experiments were designed. The first used monolayers formed from a fluorinated thiol ($CF_3(CF_2)_7(CH_2)_2SH$) and a carboxylic acid-terminated thiol ($HO_2C(CH_2)_{15}SH$). The second, described elsewhere (5), employed coatings of PMMA. Both sets of experiments used methanol as a gas phase analyte for testing performance.

The goal of the monolayer-coating experiments was to exploit the differences in the interfacial properties of the two terminal groups, thereby gaining a degree of selectivity in the adsorption of methanol vapor. Fluorinated monolayers have critical surface tensions of 5-10 mN/m (34), values indicative of a very low free surface energy. These monolayers are not wetted by methanol, and therefore should display limited affinity for the sorption of methanol vapor. Conversely, the carboxylic acid-terminated monolayer presents a much more reactive functional group at the air-monolayer interface (35). These films are wetted by methanol, a result of both the polarity and hydrogen-bonding capability of the end group. Based on wettabilities, the TFRs coated with the carboxylic acid-terminated monolayer should interact strongly with methanol, whereas those coated with the fluorinated monolayer should exhibit a lower affinity.

To test the methanol-exposure responses, TFRs were sequentially cleaned, tested with the fluorinated monolayer, cleaned, and tested with the carboxylic acid monolayer. In each run, the TFRs were equilibrated in a dry, flowing Ar atmosphere and then exposed to three different concentrations of methanol separated by flushes with Ar. Responses are shown in Figure 8A for the fluorinated monolayer and Figure 8B for the carboxylic acid-terminated monolayer. Rapid changes in $\Delta F_s/F^\circ_s$ are observed for both monolayers upon the introduction and removal of methanol from the test chamber. The responses return to their initial values upon removal of methanol, indicating that the sorption of methanol is reversible at both monolayers. The magnitude of the response of the carboxylic acid-terminated monolayer is, however, much larger than that of the fluorinated monolayer. The response differences are consistent with the behavior

predicted by wettability data, pointing to the potential use of monolayers designed for molecular recognition purposes (36, 37) as selective or class specific coatings for sensor applications. More importantly, these findings confirm the feasibility of using TFRs as mass sensors.

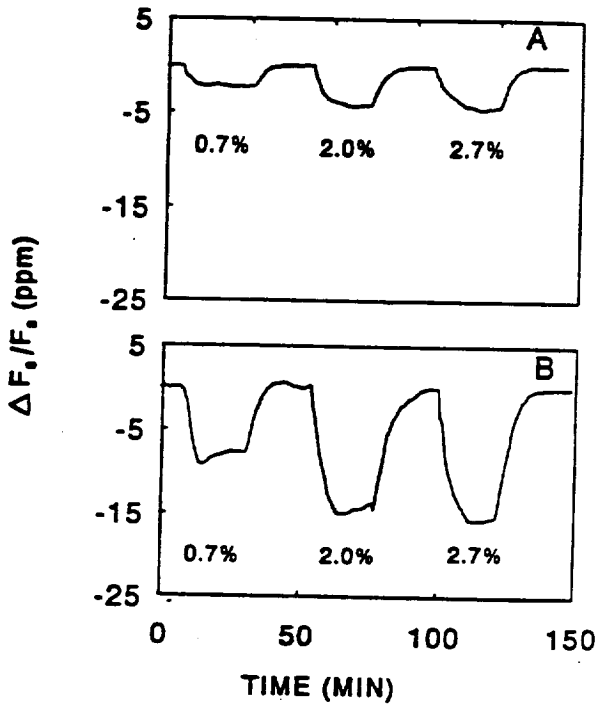

Figure 8. Baseline-corrected responses of TFRs with hydrophobic and hydrophilic surfaces to methanol. A) TFR coated with fluorinated thiolate. B) TFR coated with carboxylic acid-terminated thiolate. Responses are expressed as relative changes (i.e. $\Delta F/F^{\circ}_{s}$) using units of parts per million (ppm). Note that the response times reflect a mixture of processes, including the evaporation of methanol and the removal of methanol from the test chamber. Measurement instabilities, such as those that may arise from small temperature changes, have been accounted for using a six-point baseline linearization.

It is also interesting to note that the TFR response for both monolayers is nonlinear with methanol concentration. This behavior indicates that the surface coverage of sorbed species approaches saturation at the larger methanol concentrations. Interestingly, one can predict the saturation coverage of methanol for the carboxylic acid-terminated monolayer by assuming that each acidic functionality can bind with one methanol molecule. Since the surface coverage of these monolayers is $9.1 \pm 0.5 \times 10^{-10}$ moles/cm^2 (31, 32), the saturated coverage of methanol would translate to mass increase of 29 ng/cm^2. In Figure 8B, the maximum response of the acid-coated TFR was -12.7 ppm. This frequency change corresponds to a mass increase of 23 ng/cm^2, using the average experimental S_m value of -555 cm^2/g from Table I. Thus, it appears that the acid-terminated layer approaches a 1:1 binding stochiometry with methanol. This finding suggests that, in addition to sensor application, the TFRs may potentially find uses in fundamental studies of wetting, condensation, and a host of other important interfacial processes.

CHIP-SCALE ION CHROMATOGRAPHY

The long term goal of this project is the development of a microminiature liquid chromatograph on a silicon wafer. Such instrumentation would provide an attractive approach for environmental assessment and monitoring programs as well as the space program. Though far from completion, we envision an instrument that represents an integration of the components (e.g., injector, pump, column with chemically specific stationary phase, and detector) of conventional liquid chromatographs, though at an extreme of miniaturization. The focus of this project is several-fold. The key areas include the development of techniques for trenching small diameter (10-50 μm) columns at standard sized (76 mm) silicon wafers, for flowing solution through the columns, and for chemically modifying the walls of the columns. Each of the objectives has been accomplished to varying degrees. Trenches of the specified size have been fabricated by a combination of photolithographic and chemical etching methods. Trenches with, for example, a nominal diameter of 15 μm have been prepared, with the topography characterized by both scanning electron and atomic force microscopies. A cross-sectional view of an etched half-cylinder column is shown in Figure 9. As presented, a silicon wafer has been direct bonded to the trenched bottom-wafer to complete column fabrication. Attempts to seal two such trenches together to form a cylindrical column have met with difficulties with respect to alignment registry. Infrared imaging may overcome this difficulty.

To control the flow of solution through these columns, we have constructed a pneumatic pumping system. The pumping system provides a low flow rate (a few nL/min). The flow rate can be regulated by varying the pressure of an inert gas at the liquid in contact with the entrance channel of the column. A microelectrode, prepared by the evaporation of a small gold disk at the exit channel of the column, served as the detector for this characterization. Unexpectedly, these columns were easily plugged by small-sized particulate matter that is difficult to remove even after filtering the solutions by passage though a with a 10 μm membrane filter. We are currently devising methods to overcome this complication.

Several routes for the chemical modification of the walls of the columns have been devised, with the goal to manipulate separations in a fashion analogous to that used in conventional chromatography as well as with our recently developed electrochemically-based approach (6). The most promising approach utilizes established silane chemistry (38). In this scheme, silicon with a native oxide is exposed to an anhydrous solution containing an end-group (X) functionalized trichlorosilane ($X(CH_2)_nSiCl_3$). Through a reaction with the hydroxyl groups of the native oxide, a two-dimensional network of a cross-linked monolayer is formed.

Verification of the successful functionalization of the silicon surface with monolayers of various end-groups was obtained using infrared reflection spectroscopy and wettability measurements. These characterizations were performed on large-sized replicates of the surface of the trenched materials. We hope to report "proof of concept" in the near future.

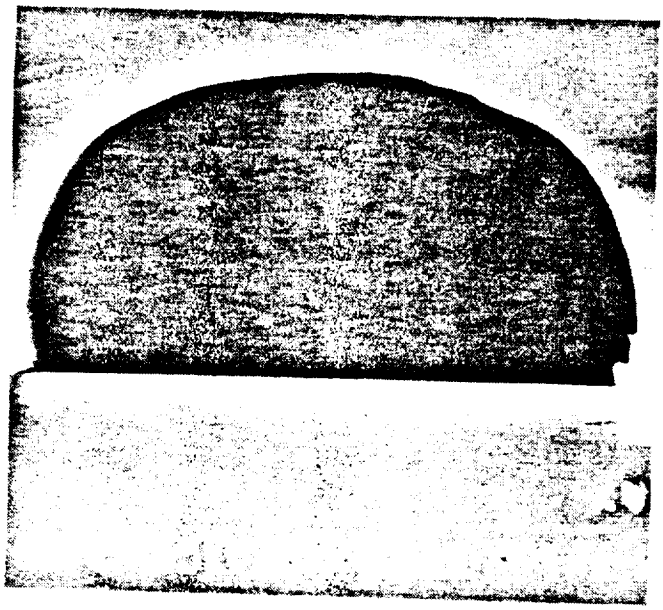

Figure 9. Scanning electron micrograph of etched trenches in silicon.

ACKNOWLEDGMENTS

M.D.P. expresses appreciation for the support of a Dow Corning Assistant Professorship, S.J.C. for a NASA/Iowa Space Grant Fellowship through the College Consortium under the NASA Space Grant Program, and R.P.O. for a Harpole Graduate Fellowship through the Department of Electrical Engineering at ISU. This work was supported in part by the Center for Advanced Technology Development at Iowa State University under USDOC Grant ITA 87-02, by the Office of Basic Energy Research-Chemical Sciences Division of USDOE, and by the Advanced Life Support Division of the NASA-Ames Research Center (Contract No. NAG2-722. Ames Laboratory is operated for the U. S. Department of Energy by Iowa State University under Contract No. W-7405-Eng-82.

REFERENCES

1. Edmonds, T. E., Ed., *Chemical Sensors*; Blackie: Glasgow, 1988.

2. Turner, A. P. F., Karube, I., Wilson, G. S., Eds., *Biosensors Fundamentals and Applications*; Oxford University Press, Oxford, 1987.

3. Janta, J. *Anal. Chem.* **1990**, *62*, 33R-44R.

4. Jones, T. P., Coldiron, S. J., Deninger, W. J. and Porter, M. D. *Appl. Spectrosc.* **1991**, *45*, 1271-77.

5. O'Toole, R. P., Burns, S. G., Bastiaans, G. J., Porter, M. D. *Anal. Chem.* **1992**, *63*, 1289-95.

6. Deinhammer, R. S., Shimazu, K., Porter, M. D. *Anal. Chem.* **1991**, *63*, 1889-94.

7. Ingle, J. D. and Crouch, S. R., *Spectrochemical Analysis*, Prentice Hall, Englewood Cliffs, New Jersey, 1988.

8. Collison, M. E. and Meyerhoff, M. E. *Anal. Chem.* **1990**, *62*, 425A-37A.

9. Jones, T. P. and Porter, M. D. *Anal. Chem.* **1988**, *60*, 404-406.

10. Stole, S. M., Jones, T. P., Lai-Kwan, C., and Porter, M. D., in *Chemical Sensors and Microinstrumentation*, Murray, R. W., Dessy, R. E., Heineman, W. R., Janta, J., and Seith, W. R., Eds: American Chemical Society Symposium Series No. 403, Washington, D.C. , 1989

11. Saari, L.A. *Anal. Chem.* **1982**, *54*, 823-4.

12. Zhujun, Z., Zhang, Y., Wangbai, M., Russell, R., Shaksher, Z. M., Grant, C. L., and Seitz, W. R. *Anal. Chem.* **1989**, *61*, 202-5.

13. Miller, W. W. *Clin. Chem.* **1987**, *54*, 823-4.

14. Webster, J. G., *Medical Instrumentation*, Houghton Mifflin Company, Boston, 1978.

15. Johnston, R. S. and Dietlein, L. F., Eds., *Biomedical Results from Skylab*, NASA SP-377, 1977.

16. Luo, S., and Walt, D. R. *Anal. Chem.* **1989**, *61*, 174-178.

17. Burns, S. G., Weber, R. J., Brayman, S. D., in *Proceedings of the 45th IEEE Symposium in Frequency Control*, **1991**, 207-11.

18. Wang, J. S., Lakin, K. M. *Appl. Phys. Lett.* **1982**, *40*, 308-10.

19. Burns, S. G., Ketcham, R. S. *IEEE Trans. Microwave Theory Tech.* **1984**, *32*, 1668-71.

20. Wang, J. S., Lakin, K. M. *IEEE Proceedings of the 1981 Ultrasonics Symposium*, 502-5.

21. Sauerbrey, G. *Z. Physik* **1959**, *155*, 206.

22. Benes, E. J. *Appl. Phys.* **1984**, *56*, 608-26.

23. Lu, C-S, Lewis, O. J. *J. Appl. Phys.* **1972**, *43*, 4384-4390.

24. Crane, R. A., Fisher, G. *J. Phys. D: Appl. Phys.* **1979**, *12*, 2019-26.

25. Kanazawa, K. K., Gordon, J. G. *Anal. Chim. Acta* **1985**, *175*, 99-105.

26. Bruckenstein, S., Shay, M. *Electrochimica Acta* **1985**, *10*, 1295-1300.

27. Beck., R., Pittermann, U., Weil, K. G. *Ber. Bunsenges. Phys. Chem.* **1988**, *92*, 1363-68.

28. Schumacher, R. *Angew Chemie*, Internat. Ed., **1990**, *29*, 329-438.

29. Wenzel, S. W., White, R. M. *Appl. Phys. Lett.* **1989**, *54*, 1976-78.

30. Bradrup, J, Immergut, E. H., Eds.; *Polymer Handbook*; Wiley, New York, 1975, 2nd Ed.

31. Widrig, C. A., Chung, C., Porter, M. D. *J. Electroanal. Chem.* **1991**, *113*, 2805-10.

32. Walczak, M. M., Popenoe, D. D., Deinhammer, R. S., Lamp, B. D., Chung, C., Porter, M. D. *Langmuir* **1991**, *7*, 2687-93.

33. Krishnaswamy, S. V., Rosenbaum, J., Horwitz, S., Vale, C., Moore, R. A. *IEEE Proceed. 1990 Ultrasonics Symposium*, New York, **1990**, 529-36.

34. Shafrin, E. G., Zisman, W. A. *J. Phys. Chem.* **1960**, *64*, 519-28.

35. Whitesides, G. M., Laibinis, P. E. *Langmuir* **1990**, *6*, 87-96.

36. Rubenstein, I., Steinberg, S., Yitzhak, T., Shanzar, A., Savig, J. *Nature* **1988**, *332*, 426-29.

37. Arduengo, A. J., Moran, J. R., Rodriguez-Parada, J., Ward, M. D. *J. Am. Chem. Soc.* **1990**, *112*, 6153-54.

38. Netzer, L., Sagiv, J. *J. Am. Chem. Soc.* **1983**, *105*, 674-81.

39. Wohltjen, H., Snow, A. W., Barger, W. R., Ballantine, D. S. *IEEE Trans. Ultrasonics. Ferroelectric Freq. Control* **1987**, *343*, 172-78.

40. Grate, J. W., Klusty, M. *Anal. Chem.* **1991**, *63*, 1719-1727.

Sensitivity Mass Sensors

ANAL. CHEM. in press.

Ronald P. O'Toole,[†,‡] Stanley G. Burns,[†,‡] Glenn J. Bastiaans,[*,§,∥] and Marc D. Porter[*,‡,§,∥,⊥]

Department of Electrical Engineering and Computer Engineering, Microelectronics Research Center, Center for Advanced Technology Development, Center for Microanalytical Instrumentation, Ames Laboratory–USDOE, and Department of Chemistry, Iowa State University, Ames, Iowa 50011

A miniaturized piezoelectric mass sensor has been developed that displays a very high mass sensitivity, S_m. The sensor is based upon thin film resonator (TFR) technology,[1] which is used to produce a gold-coated thin film (5.5 μm) resonator (TFR) of piezoelectric aluminum nitride in the shape of 400-μm squares. At this thickness, the TFRs support a standing bulk acoustic wave in a longitudinal mode at frequencies of ~1 GHz. Coatings of poly(methyl methacrylate) and spontaneously adsorbed monolayers from alkanethiols ($CH_3(CH_2)_nSH$, n = 3, 17) were used for the evaluation of S_m. Results indicated that the S_m (~−550 cm²/g) of the TFRs rivals those of the most sensitive mass sensors currently available, while offering such performance in a markedly smaller device. Coatings were also used to sorb a gaseous analyte (i.e. methanol) at the TFRs to test their potential as gas-phase sensors. Tests conducted using monolayers formed by the chemisorption of a fluorinated thiol ($CF_3(CF_2)_7(CH_2)_2SH$) and an acid-terminated thiol ($HO_2C(CH_2)_{15}SH$) at the gold electrodes demonstrated both the performance of the TFRs and a primitive manipulation of the sorption selectivity of the interfacial structure. Possible applications of the TFRs as mass sensors are examined based upon their high mass sensitivity and compatibility for device integration using semiconductor processing technology.

INTRODUCTION

The explosive growth in chemical sensor research is being driven largely by the increasing technological need to perform analytical measurements remote from a central laboratory.[2-7] Environmental monitoring, process control, and bedside patient monitoring serve as examples of such needs. Though specific attributes are application dependent, there is a general consensus that such sensors be compact, yield quantitative information, and have responses specific to a given analyte or classes of analytes. It is also desirable that the sensors be fabricated at low cost to enhance their deployment in large numbers or as consumables (i.e., with limited operational lifetimes).

One class of sensors with the potential to meet the above requirements is the piezoelectric mass sensor.[4,7-12] Such sensors exhibit a response at low loading levels that is proportional to the mass of a sorbed analyte. Sensors based on mass changes have been applied to the detection of a variety of analytes in both gas[9,10] and solution[4,12] phases. Detection at trace levels has been obtained in several cases,[9,10,13] with specificity generally achieved via the affinity of an analyte to a coating deposited on the surface of the sensor. Hence, the development of coatings that can selectively discriminate between possible analytes is critical to meet the demands of many of the noted applications. It is also important to note that piezoelectric mass sensors have proven useful in fundamental studies of surface chemistry, with the high mass sensitivity exploited to monitor kinetics and thermodynamics of adsorption, electrode reactions, and other interfacial processes.[7,12,13-18]

We introduce a new form of piezoelectric mass sensor in this paper. The sensor is based on thin film resonator (TFR) technology.[1,19-22] The sensor has a high mass sensitivity, (S_m, ~550 cm²/g), is small in size, is easily fabricated, and can potentially be mass-produced at low cost. The sensor is a thin film bulk acoustic wave resonator, which consists of an oriented AlN membrane situated between two metal electrodes. Using microlithographic techniques, gold-coated TFRs were produced as 400-μm squares. Such small sizes open the possibility of integrating as many as 200 TFRs and associated support electronics onto a single 76-mm-diameter silicon wafer. The membrane thicknesses (5.5 μm) lead to resonance frequencies of ~1 GHz. As will be demonstrated, these high-resonance frequencies translate to mass sensitivities that rival those of the most sensitive piezoelectric mass

* Authors to whom correspondence should be addressed.
† Department of Electrical Engineering and Computer Engineering.
‡ Microelectronics Research Center.
§ Center for Advanced Technology and Development.
∥ Center for Microanalytical Instrumentation.
⊥ Ames Laboratory–USDOE and Department of Chemistry.

(1) Lakin, K. M.; Wang, J. S.; Landin, A. R. *Proceedings of the 36th Annual Symposium on Frequency Control* 1982, 517-524.
(2) Edmonds, T. E., Ed. *Chemical Sensors*; Blackie: Glasgow, 1988.
(3) Madou, M. J.; Morrison, S. R.; *Chemical Sensing with Solid State Devices*; Academic Press: New York, 1989.
(4) Bastiaans, G. J. In *Chemical Sensor Technology*; Yamazoe, N., Ed. Elsevier: Amsterdam; Vol. 4, 1992; pp 181-204.
(5) Turner, A. P. F., Karube, I., Wilson, G. S., Ed. *Biosensors Fundamentals and Applications*; Oxford University Press: Oxford, 1987.
(6) Janata, J. *Anal. Chem.* 1990, *62*, 33R-44R.
(7) Ward, M. D.; Buttry, D. A. *Science* 1990, *249*, 1000-1007.
(8) McCallum, J. J. *Analyst* 1989, *114*, 1173-1189.
(9) Guilbault, G. G.; Jordan, J. M. *CRC Crit. Rev. Anal. Chem.* 1988, *19*, 1-28.
(10) Fox, C. G.; Alder, J. F. *Analyst* 1989, *114*, 997-1004.
(11) Grate, J. W.; Wenzel, S. W.; White, R. M. *Anal. Chem.* 1991, *63*, 1552-1561.
(12) Schumacher, R., *Angew Chem., Int. Ed. Engl.* 1990, *29*, 329-438.
(13) Zellers, E. T.; White, R. M. Rappaport, S. M. *Anal. Chem.* 1990, *62*, 1222-1227.
(14) Buttry, D. A. In *Electroanalytical Chemistry*; Bard, A. J., Ed.; Marcel Dekker: New York, 1991; Vol. 15.
(15) Wholtjen, H.; Dessy, R. E. *Anal. Chem.* 1979, *51*, 1470.
(16) Ballantine, D. S.; Wohltjen, H.; In *Chemical Sensors and Microinstrumentation*; Murray, R. W., Ed.; ACS Symposium Series 403; American Chemical Society: Washington, DC, 1989; pp 222-236.
(17) Frye, G. C.; Martin, S. J.; Ricco, A. J.; Brinker, C. J. *In Chemical Sensor and Microinstrumentation*; Murray, R. W., Ed.; ACS Symposium Series 403; American Chemical Society: Washington, DC, 1989; pp 208-221.
(18) Thomas, R. C.; Sun, Li; Crooks, R. M.; Ricco, A. J. *Langmuir* 1991, *7*, 620-622.
(19) Burns, S. G.; Weber, R. J.; Brayman, S. D. In *Proceedings of the 45th IEEE Symposium in Frequency Control* 1991, 207-211.
(20) Wang, J. S.; Lakin, K. M. *Appl. Phys. Lett.* 1982, *40*, 308-310.
(21) Burns, S. G.; Ketcham, R. S. *IEEE Trans. Microwave Theory Tech.* 1984, *32*, 1668-1671.
(22) Wang, J. S.; Lakin, K. M. *IEEE Proceedings of the 1981 Ultrasonics Symposium*, 1981, 502-505.

0003-2700/xx/0300-0001$03.00/0

This paper is the first of a series that will address issues related to device design and system integration, electronic measurement techniques, selective coatings, and performance characteristics of this new form of mass sensor. We report here the results of feasibility studies which have defined experimental measurement protocols, established currently achievable mass sensitivities, and demonstrated the potential of TFRs as the transducer component in a gas-phase chemical sensor. The mass-sensitivity evaluations and transducer demonstrations were conducted using thin organic films of poly(methyl methacrylate), PMMA, and spontaneously adsorbed monolayer films formed by the chemisorption of thiol compounds with different tail groups (i.e., $CH_3(CH_2)_3SH$, $CH_3(CH_2)_{17}SH$, $HO_2C(CH_2)_{15}SH$, and $CF_3(CF_2)_7(CH_2)_2SH$). Methanol was used as the test sorbant.

THEORY

Piezoelectric mass sensors are passive solid-state electronic devices that respond to changes in temperature, pressure, and, most importantly, the physical properties of the interface between the surface and a contacting medium. Such changes include interfacial mass density, elasticity, viscosity, and sorbed layer thickness. This type of sensor operates by monitoring the propagation of an acoustic wave through the solid-state device. The more common mass sensor is an acoustic bulk wave resonator which is constructed by applying metal electrodes to the surfaces of a thin piezoelectric plate or membrane. Variations in, for example, the composition of the interface between the resonator and the surrounding medium, are reflected by changes in the resonance frequency of the acoustic wave.

Sauerbrey first demonstrated that acoustic bulk wave resonators could be used as mass sensors.[23] As indicated by the classic Sauerbrey equation, the change in series resonance frequency is linearly related to the mass of a material sorbed on a resonator surface.[23,24] Three equivalent forms of the classic Sauerbrey equation are

$$\frac{\Delta F_s}{F_s^0} = \frac{-\rho_l D_l}{\rho_s D_s} \tag{1a}$$

$$\frac{\Delta F_s}{F_s^0} = \frac{-2F_s^0 \rho_l D_l}{(\rho_s C_s)^{1/2}} \tag{1b}$$

$$\frac{\Delta F_s}{D_s^0} = \frac{-2F_s^0 \Delta M}{(\rho_s C_s)^{1/2}} \tag{1c}$$

where ρ_l is the density of the deposited layer, ρ_s is the density of the resonator material (substrate), D_l is the thickness of the deposited layer, D_s is the thickness of the resonator, F_s^0 is the initial series resonance frequency, ΔF_s is the change in series resonance frequency after the deposition of the material, C_s is the stiffness constant of the substrate, and ΔM represents the change in mass per unit surface area arising from analyte sorption. A negative sign on the right-hand side of eqs 1a–c indicates that the series resonance frequency, F_s, decreases with increases in mass load. It is also important to note that eqs 1a–c are accurate only for mass depositions less than 2% of the actual mass of the resonator.[24] Equations 1a–c also neglect the effects of differences in the elasticity and/or viscosity of the sorbed material with respect to the resonator depositions[24-26] and between elasticity and viscosity changes.[12,27-29]

The mass sensitivity, S_m, of a piezoelectric mass sensor can be defined, as shown by Wenzel and White,[30] as

$$S_m = \lim_{\Delta m \to 0} \left(\frac{\Delta F_s}{F_s^0}\right)\left(\frac{1}{\Delta M}\right) \tag{2}$$

By applying eq 2 to the Sauerbrey model, the following theoretical expression for S_m was derived for a bulk acoustic wave resonator:[30]

$$S_m = \frac{-n}{\rho_s D_s} \tag{3a}$$

where n is an integer designating the resonance mode. An equivalent form of this expression relates S_m to n, F_s^0, ρ_s, and the velocity (V) of the acoustic wave, and is written as

$$S_m = -\frac{2nF_s^0}{\rho_s V} \tag{3b}$$

Since S_m is inversely proportional to resonator thickness, the AlN TFRs are predicted to have an extremely high mass sensitivity (see Table I).

In most sensor applications, an approximation of F_s is obtained by measuring the frequency of an oscillator circuit that incorporates the resonator in a two-port device configuration as the frequency-determining element in the feedback loop of an amplifier. In such circuits, the oscillation frequency, F_o, corresponds to the frequency where the phase shift across the entire feedback loop is $2\pi N$, where $N = 0, 1, 2$.[33] The electrical behavior of a resonator is best illustrated by examining an admittance diagram as shown in Figure 1A. The admittance circle is a plot of susceptance, B, vs conductance, G (i.e., the real and imaginary components of admittance), of the resonator as a function of frequency following the resonator equivalent circuit of Figure 1B. A zero phase shift across the resonator occurs when the magnitude of susceptance is zero. The high conductance crossing of the x axis by the circle is defined as the resonance frequency, F_r. In general, phase shifts in the feedback loop are sufficiently small such that oscillation occurs near zero resonator phase shift and F_o approximates F_r. However, the total phase shift in the oscillator feedback loop is a function of the intrinsic properties of the resonator, the amplifier, physical or chemical perturbations of the resonator, and parasitic capacitive or other reactive circuit elements. The latter would result from mechanical mounting and circuit connections. Thus, the oscillation frequency often observed with piezoelectric mass sensors is susceptible to variations of electronic and mechanical components that are not related to changes in F_s of the sensor. It is also possible that certain operating conditions (e.g., high interfacial viscosity) can lead

(23) Sauerbrey, G. *Z. Physik* **1959**, *155*, 206.
(24) Benes, E. J. *Appl. Phys.* **1984**, *56*, 608–626.
(25) Lu, C.-S.; Lewis, O. *J. Appl. Phys.* **1972**, *43*, 4384–4390.
(26) Crane, R. A.; Fischer, G. *J. Phys. D: Appl. Phys.* **1979**, *12*, 2019–2026.
(27) Kanazawa, K. K.; Gordon, J. G. *Anal. Chim. Acta* **1985**, *175*, 99–105.
(28) Bruckenstein, S.; Shay, M. *Electrochim. Acta* **1985**, *10*, 1295–1300.
(29) Beck, R.; Pittermann, U., Weil, K. G. *Ber. Bunsenges. Phys. Chem.* **1988**, *92*, 1363–1368.
(30) Wenzel, S. W.; White, R. M. *Appl. Phys. Lett.* **1989**, *54*, 1976–1978.
(31) Wohltjen, H.; Snow, A. W.; Barger, W. R.; Ballantine, D. S. *IEEE Trans. Ultrason. Ferroelectric Freq. Control* **1987**, *343*, 172–178.
(32) Grate, J. W.; Klusty, M. *Anal. Chem.* **1991**, *63*, 1719–1727.
(33) Smith, W. L. In *Precision Frequency Control, Vol. 2, Oscillators and Standards*; Gerber, E. A., Ballato, A., Eds.; Academic Press: New York, 1985; Chapter 8.

Table I. Performance Characteristics of Various Piezoelectric Mass Sensors

device	operating frequency (MHz)	S_m (cm²/g) calcd	S_m (cm²/g) exptl	ref
quartz crystal microbalance	6	−14	−14	25
surface acoustic wave	112	−151	−91	31
	200	−252	−263	32
	400	−505	−493	32
flexural plate	2.6	−951	−990	30
	5.5		−379	11

thin film resonators (resonator No.)			PMMA loading[a]	
63C-H9	957		−563	−463
63C-H12	955		−562	−445
63C-J11	945		−556	−514
63C-J12	951		−559	−574
63C-M11	989		−582	−630
63D-H8	946		−556	−469
63D-J6	989		−582	−613
63D-J12	949		−558	−435
63D-L7	1000		−588	−440
		av	−567	−509
			monolayer loading[b]	
63C-L9	973		−572	−753
63C-M11	989		−582	−728
63C-J7	983		−578	−464
		av	−574	−555

[a] PMMA loading experiments used preparative conditions yielding a film thickness of 21.7 ± 0.7 nm. [b] Monolayer loading experiments were conducted in a differential mode and are based on the changes in F_s for films formed by the spontaneous adsorption of $CH_3(CH_2)_3SH$ and $CH_3(CH_2)_{17}SH$.

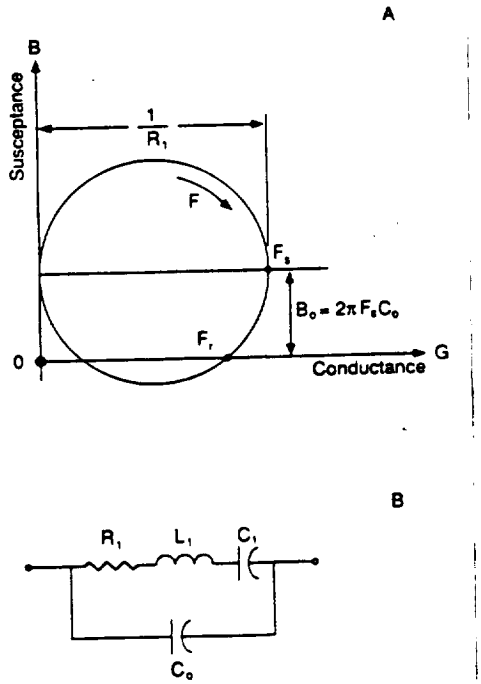

Figure 1. (A) Plot of electrical susceptance vs conductance as a function of frequency for a bulk wave resonator. The admittance circle has diameter of $1/R_1$. B_0 is the displacement of the center of the circle from the x axis. (B) Butterworth–Van Dyke equivalent circuit for a bulk wave resonator. C_0 is the parasitic capacitance. L_1, R_1, and C_1 are the inherent motional arm equivalent circuit parameters for the resonator.

to a loss of oscillation.[34] In practice, however, F_o is often an acceptable measure of response if unwanted sources of frequency variation and energy loss can be made small relative to the amplitude of the analytical response.

(34) Kipling, A. L.; Thompson, M. *Anal. Chem.* **1990**, *62*, 1514–1519.

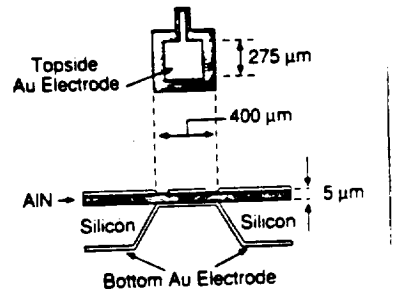

Figure 2. Schematic diagrams of a thin film resonator. The upper portion is a top view where the Au electrode is shown in white and the underlying AlN membrane is shown by the hatch-markings. The lower portion is a side view which illustrates the layered structure of the composite material.

For sensor development purposes, a more ideal approach is to measure directly the series resonance (sometimes referred to as motional arm resonance) frequency of the device, i.e., F_s. By definition, F_s is the frequency of maximum conductance for a resonator.[35,36] This frequency is solely dependent on the intrinsic properties of the resonator and is not affected by the addition of other series or parallel circuit elements.[36] The determination of F_s can be done by measuring the electrical admittance characteristics of the resonator over a range of frequencies centered about F_s. By plotting electrical susceptance versus conductance over the observed frequency range, all or part of the characteristic admittance circle of the resonator can be determined. The point of maximum conductance on this circle corresponds to F_s, as shown in Figure 1A. The value of F_s can be accurately computed with high precision by fitting the experimental data to a circle function using a least squares computation.[36]

It is important, however, that F_s not be confused with F_r which, as defined earlier, equals the frequency of zero phase shift at high conductance. The value of F_r can also be found from an admittance plot but can be influenced by circuit elements not intrinsic to the resonator. For example, variations in the parasitic capacitance, C_o (see Figure 1B), will cause a vertical shift in the position of the admittance circle and induce a change in F_r not related to the mass response of the sensor. In addition, changes in acoustical losses (i.e., damping) of the resonator will cause a change in the diameter of the admittance circle, leading to a change in F_r. In contrast, changes in C_o or acoustical losses do not influence F_s.

Accurate measurements of F_s and F_r require specialized electronic test equipment such as vector voltmeters or network analyzers with precise frequency synthesizers. As a consequence, the measurement of F_s or F_r is not practical for routine sensor applications. However, F_s or F_r should be meausred during the design and testing phase of sensor development.[34] Such measurements provide a more detailed characterization of the resonator properties, and in some instances, may lead to insights into possible sources of systematic measurement errors.

EXPERIMENTAL SECTION

TFR Fabrication. Figure 2 shows a cross-sectional and top view of an AlN TFR. The AlN membrane is produced by depositing Al in a low-pressure N_2 atmosphere onto a Si substrate using a dc magnetron sputtering system.[1] The "topside" electrode is prepared by the sequential deposition of thin Ti (~20 nm) and

(35) *Standard Methods for Measurement of the Equivalent Electrical Parameters of Quartz Crystal Units, 1kHz to GHz, EIA-512*; Electronic Industries Association: Washington, DC, 1985.

(36) Hafner, E. In *Precision Frequency Control, Vol. 2, Oscillators and Standards*; Gerber, E. A., Ballato, A., Eds.; Academic Press: New York, 1985; Chapter 7.

Au (~200 nm) films onto the AlN membrane, with Ti acting as an adhesive layer between Au and the native oxide of Si. Microlithography techniques are then used to pattern the electrodes as 400-μm squares.

The "backside" electrodes are made by etching Si from beneath the AlN membrane. After etching, the electrodes are laid down by the sequential deposition of Ti and Au layers with thicknesses comparable to those of the topside electrode. The backside electrodes also serve as a ground plane. Using this procedure, TFRs with thicknesses of 5.5 ± 0.5 μm have been prepared. Further details of the fabrication procedure[1] and supporting information[18-22] have been described elsewhere.

It is also important to note that the *c* axis of the AlN membrane is oriented normal to the Si surface, providing a TFR for gas sensor applications. As a consequence, an oscillating electrical field at the resonator electrodes produces an acoustic wave that is predominantly longitudinal in character. Procedures for orienting AlN to produce shear waves suitable for sensing in liquids have also been devised.[37]

Electrical Measurements. The TFRs were coated and tested in the form of whole 76-mm-diameter wafers. Electrical contact was made using a set of rf probes mounted on a micropositioner (Cascade Microtech). One-port scattering parameters (*S* parameters) were measured using either a Hewlett-Packard 8510 or 8753 network analyzer. The *S* parameters relate the voltage waves incident on the port of those reflected from the port. Automated data acquisition and analysis were achieved using Hewlett-Packard 85165A resonator measurement software running on either an HP-236 computer workstation or an HP-8234A measurement co-processor. The software transforms the measured scattering parameters to electrical admittance values. The program uses the Butterworth–Van Dyke equivalent circuit model to fit the data to an admittance circle and then calculates F_s. Results reported as changes in F_r were measured at the frequency at which the susceptance is zero. An estimate of the uncertainty of a measurement of relative frequency was obtained by determining repetitively $\Delta F_r/F_r^0$ at 2-min intervals under quiescent conditions. The standard deviation calculated from several such measurements was 0.3 ppm.

Preparation of Polymer and Monolayer Films. Thin PMMA (Aldrich) films were cast onto the TFRs by spin-coating techniques. These films were prepared from a 0.25% (w/v) solution of chlorobenzene and were soft-baked at 85 °C. This procedure resulted in film thicknesses of 21.7 ± 0.7 nm as determined via optical ellipsometry.

The TFRs were also coated with monolayers formed by the chemisorption of thiol-containing compounds onto the gold electrodes.[38-40] These monolayers spontaneously adsorb as densely packed structures from dilute solution as the corresponding thiolate[41] and have been extensively studied as models for probing fundamental details of heterogeneous electron-transfer,[42-43] wetting,[39] and a variety of other interfacial processes.[39] Four structurally distinct monolayers were prepared: a short- ($CH_3(CH_2)_4S^-$) and long-chain ($CH_3(CH_2)_{17}S^-$) alkanethiolate, a highly fluorinated ($CF_3(CF_2)_7(CH_2)_2S^-$) thiolate, and an acid-terminated ($HOOC(CH_2)_{15}S^-$) thiolate. The long- and short-chain alkanethiolates are used in the mass sensitivity determination and provide a surface coverage of (9.1 ± 0.5) × 10^{-10} mol/cm^2.[41,44] The fluorinated and acid-terminated thiolates are utilized in demonstrating the potential application of the TFRs as a gas-phase sensor. The alkanethiols were obtained from Aldrich. The fluorinated thiol was a gift from Dr. Fred Behr. The acid-terminated thiol was a gift from Professor George Whitesides.

Prior to the formation of thiolate layers, the gold surfaces of the TFRs were cleaned to remove any residual materials from lithographic processing and other handling procedures. For cleaning, the TFRs were placed in a dilute solution of I_2/KI (2.3 g of KI and 1.3 g of I_2 in 1 L of H_2O) for ~30 s, a process that etched away several atomic layers of the gold surface. Residual materials were removed by rinsing freshly etched surfaces in a solution of 1:3 H_2O_2(30%)–H_2SO_4(concd) for 1–2 min. **Caution:** *The H_2O_2/H_2SO_4 solution reacts violently with organic compounds and should be handled with extreme care.* Following thorough rinses with H_2O and ethanol, the thiolate monolayers are formed by immersing the TFRs in a 1–5 mM ethanolic solution of the corresponding thiol from 5 min up to ~12 h. As earlier studies have shown,[39] these monolayers form within a few minutes; longer immersion times were used primarily for convenience. Upon removal from solution, the TFRs were rinsed in ethanol and hexane and dried in air.

Ellipsometric Measurements of Film Thickness. The thicknesses of the PMMA films were determined by optical ellipsometry in two steps using a computer-controlled Gaertner Model L-116B ellipsometer at 632.8 nm. The incident angle was 70° from the surface normal. After plasma treatment, the analyzer and polarizer angles for a reflected light beam from each uncoated sample were measured on at least four different spots. The average complex refractive index for the substrate was then calculated with a two-phase parallel layer model from classical electromagnetic theory.[45] After coating, the samples were again analyzed and the film thickness calculated from a three-phase parallel layer model using the average complex refractive index of each uncoated sample and the real refractive index of PMMA (1.42[46]).

Adsorption Testing. The TFRs and rf probe assembly were enclosed during testing in a large-volume (~9-L) Plexiglas chamber to allow controlled introduction of analyte. The large-size chamber, which complicated the gas sorption tests, facilitated mounting and connecting the individual TFRs to the rf probes. Methanol was introduced into the chamber as a liquid with a syringe through an injection port onto a glass dish. Measured volumes of methanol were injected and allowed to evaporate completely, yielding a known vapor concentration. Between methanol injections, the chamber was purged exhaustively with Ar.

RESULTS AND DISCUSSION

To evaluate the feasibility of using TFRs as gas-phase chemical sensors, the responses to coating application and to exposure to methanol vapor after coating application were experimentally observed. Responses were measured as changes in F_s or F_r before and after coating or exposure to methanol; these two parameters were found to be equivalent under our test conditions. Responses are expressed as relative changes (e.g., $\Delta F_s/F_s^0$) using units of parts per million (ppm).

Mass Sensitivity (S_m). The sensitivity of the TFRs to mass loading was determined by two different experiments. The first monitored the effect of the deposition of a 21.7 ± 0.7 nm film of PMMA on the resonator properties. Measurements were taken on several TFRs with typical absolute and relative frequency changes after coating of 35 kHz and 39 ppm, respectively. Based on the coating thickness and the density of bulk PMMA (1.2 g/cm^3),[47] the mass of deposited material per unit area (ΔM) was calculated.

In the second experiment, the resonator properties were first measured for TFRs coated with a butanethiolate monolayer. The TFRs were then cleaned, coated with a monolayer of octadecanethiolate, and tested. The relative difference in the two values of F_s was taken as the response to the change in mass loading between the two different chain length

(37) Wang, J. S.; Landin, A. R.; Landin, A. R. *Proceedings of the 36th Annual Symposium on Frequency Control* 1983, 491–494.
(38) Porter, M. D.; Bright, T. B.; Allara, D. L.; Chidsey, C. E. D. *J. Am. Chem. Soc.* 1987, *109*, 3559–3568.
(39) Whitesides, G. M.; Laibinis, P. E. *Langmuir* 1990, *6*, 87–96.
(40) Nuzzo, R. G.; Duboid, L. H.; Allara, D. L. *J. Am. Chem. Soc.* 1990, *112*, 558–569.
(41) Widrig, C. A.; Chung, C.; Porter, M. D. *J. Electroanal. Chem. Interfacial Electrochem.* 1991, *113*, 2805–2810.
(42) DeLong, H.; Buttry, D. A. *Langmuir* 1990, *6*, 1319–1322.
(43) Chidsey, C. E. D.; *Langmuir*, 1991, *251*, 919–922.
(44) Walczak, M. M.; Popenoe, D. D.; Deinhammer, R. S.; Lamp, B. D.; Chung, C.; Porter, M. D. *Langmuir* 1991, *7*, 2687–2693.
(45) Allara, D. L.; Nuzzo, R. G. *Langmuir* 1985, *1*, 45–52.
(46) Allara, D. L.; Baca, A.; Pryde, C. A. *Macromolecules* 1978, *11*, 1215–1220.
(47) Brandrup, J., Immergut, E. H., Eds. *Polymer Handbook*, 2nd ed.; Wiley: New York, 1975.

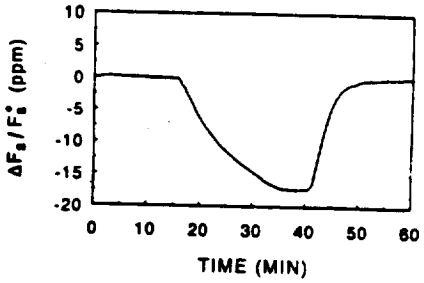

Figure 3. Baseline-corrected frequency response to a PMMA-coated TFR to methanol exposure (2.68% v/v).

monolayers. Since both the butanethiolate and octadecanethiolate monolayers form low surface tension interfacial structures with comparable surface coverages [$(9.1 \pm 0.5) \times 10^{-10}$ mol/cm^2 [41,44]], the difference in mass loading between the two thiolate monolayers was calculated from their molecular weight differences. Such tests using uncoated TFRs are impractical because of contaminant adsorption onto the "bare" gold surface.

From the results of the two different mass loading experiments, values of S_m were calculated using eq 2. Equation 3b was used to compute a S_m value based on the value of F_s^0 and the literature values of ρ_s and V.[48] Table I summarizes the results and provides related data for other forms of piezoelectric mass sensors for comparison. As is evident, the average experimentally determined values of S_m (−509 and −555 cm^2/g) are comparable to those predicted by theory (−567 and −574 cm^2/g). More importantly, these results show that the TFRs exhibit a much greater intrinsic sensitivity to mass loading than the QCMs. Only the flexural plate and the high-frequency SAW devices, which are both markedly larger in size and have much more complex electrode patterns, have comparable sensitivities.

Demonstration of Performance of TFRs as a Gas-Phase Sensor. As is the case for many types of chemical sensors, the performance of piezoelectric mass sensors is as much or more a function of the surface coating as it is of the mass response characteristics. The properties of the coating determine the rate of the response, reversibility, and selectivity. The coatings also play a major role in defining the relationship between analyte concentration and analytical response. Therefore, the choice of the coating is one of the most critical aspects of sensor design. To demonstrate the feasibility of using TFRs as sensors, two relatively simple sets of experiments were designed. The first employed coatings of PMMA. The second used monolayers of the fluorinated thiolate and the carboxylic acid-terminated thiolate. Both sets of experiments used methanol as a gas-phase analyte for testing performance.

In the first set of experiments, TFRs coated with a 21.7 ± 0.7 nm film of PMMA were exposed to methanol vapor. The vapor chamber was flushed thoroughly with Ar between successive additions to remove methanol from the previous sample. Figure 3 indicates the time-dependent response typically observed for the TFR coated with PMMA. Upon flushing the chamber with Ar, the response of the TFR returned to its original amplitude before exposure to methanol. This behavior indicates that the PMMA coating acts as a reversible sorbant of methanol. It is important to note that the response times reflect a mixture of processes, including the evaporation of methanol, the permeation of methanol in PMMA, and the removal of methanol from the test chamber.

Response amplitudes from a series of injections of different volumes of methanol were found to be linear over the range

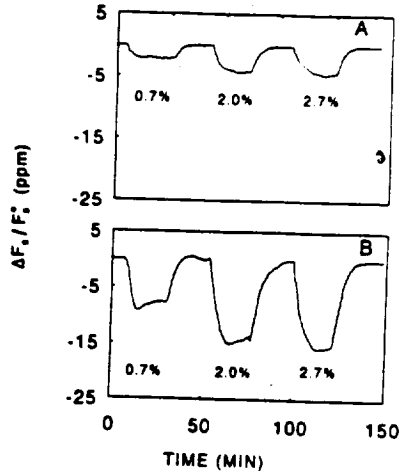

Figure 4. Baseline-corrected responses of TFRs with hydrophobic and hydrophilic surfaces to methanol. (A) TFR coated with fluorinated thiolate. (B) TFR coated with carboxylic acid-terminated thiolate.

of methanol concentrations tested (1% to 7% (v/v)), indicating that the mass of vapor sorbed was proportional to methanol vapor phase concentration. The plot of $\Delta F_s/F_s^0$ (ppm) vs percent methanol gave a slope of −5.65 and a y-intercept of 0.31; the correlation coefficient was 0.99. This set of responses is also consistent with that expected by the Sauerbrey equation for a well-behaved mass sensor.

In the second set of experiments, a somewhat more sophisticated approach was taken for demonstrating feasibility. These experiments employed TFRs that were coated with a monolayer of the fluorinated thiolate ($CF_3(CF_2)_7(CH_2)_2S^-$) and the carboxylic acid-terminated thiolate ($HOOC(CH_2)_{15}S^-$). The goal was to exploit the differences in the interfacial properties of the two layers, thereby gaining a degree of selectivity in the adsorption of methanol vapor. The fluorinated monolayer is expected to have a critical surface tension of 5–10 mN/m,[49] values indicative of a very low free surface energy. These monolayers are not wetted by methanol. As such, this monolayer should display limited affinity for the sorption of methanol vapor. Conversely, the carboxylic acid-terminated monolayer presents a much more reactive functional group at the air–monolayer interface.[39] These films are wetted by methanol, a result of both the polarity and hydrogen-bonding capability of the end group. On the basis of wettabilities, one would then predict TFRs coated with the carboxylic acid-terminated thiolate to interact strongly with an analyte such as methanol, whereas those coated with the fluorinated thiolate to exhibit a lower affinity.

To test the above response predictions, TFRs were sequentially cleaned, tested with the fluorinated thiolate coating, cleaned, and tested with the carboxylic acid thiolate coating. In these tests, the TFRs were allowed to equilibrate in a dry, flowing Ar atmosphere to establish a baseline response prior to analyte injection. The TFRs were then exposed to three different concentrations of methanol separated by flushes with Ar. Representative responses from such tests are shown in Figure 4A for the fluorinated thiolate and Figure 4B for the carboxylic acid-terminated thiolate. These data are summarized in Table II. Measurement instabilities, such as those that may arise from small temperature changes, have been accounted for using a six-point baseline linearization. Rapid changes in $\Delta F_s/F_s^0$ are observed for both monolayers upon the introduction and removal of methanol from the test chamber. The responses return to their baseline corrected values upon removal of methanol, indicating that the sorption of methanol is essentially reversible at both monolayers. The magnitude of the responses of the two monolayers are,

(48) Krishnaswamy, S. V.; Rosenbaum, J.; Horwitz, S.; Vale, C.; Moore, R. A. *Proceedings of the 1990 Ultrasonics Symposium*; IEEE: New York, 1990; pp 529–536.

(49) Shafrin, E. G.; Zisman, W. A. *J. Phys. Chem.* 1960, *64*, 519–528.

Table II. Frequency Responses (ppm)[a] and Mass Changes (ng/cm²) of TFRs Coated with Fluorinated ($CF_3(CF_2)_7(CH_2)_2S^-$) and a Carboxylic Acid-Terminated ($HO_2C(CH_2)_{15}S^-$) Thiolate Monolayers upon Exposure to Methanol Vapor

methanol concn (% (v/v))	$CF_3(CF_2)_7(CH_2)_2S$/Au		$HO_2C(CH_2)_{15}S$/Au	
	$\Delta F_s/F_s^0$	ΔM	$\Delta F_s/F_s^0$	ΔM
0.0	0.0	0.0	0.0	0.0
0.67	−1.4	2.5	−5.8	10.5
2.01	−2.9	5.3	−12.6	22.7
2.68	−3.3	6.0	−12.7	22.8

[a] Uncertainties are 0.3 ppm (see the Experimental Section for details of the determination of the uncertainty).

however, notably different, with that of the carboxylic acid-terminated thiolate being much larger than that of the fluorinated thiolate. These response differences are consistent with the behavior predicted by wettability data, pointing to the potential use of thiolate monolayers designed for molecular recognition purposes[50,51] as selective or class-specific coatings for sensor applications. More importantly, these findings confirm the feasibility of using TFRs as mass sensors.

It is also interesting to note that the relationship between the TFR response and methanol concentration is nonlinear for both monolayers. This behavior indicates that the surface coverage of sorbed species approaches saturation at the larger methanol concentrations. One can predict the saturation coverage of methanol, for example, for the carboxylic acid-terminated monolayer by assuming that each acidic functionality can bind with one methanol molecule. Since the surface coverage of thiolates at gold is $9.1 \pm 0.5 \times 10^{-10}$ moles/cm² (41,44), the saturated coverage of methanol would translate to a mass increase of 29 ng/cm². In Figure 4B, the maximum response of the acid-coated TFR was −12.7 ppm. This frequency change corresponds to a mass increase of 23 ng/cm², using the average experimental S_m value of −555 cm²/g from Table I. Thus, it appears that the acid-terminated layer approaches a 1:1 binding stoichiometry with methanol. This finding suggests that, in addition to sensor applications, the TFRs may potentially find uses in fundamental studies of wetting, condensation, and a host of other important interfacial processes.

(50) Rubenstein, I.; Steinberg, S.; Yitzhak, T.; Shanzar, A.; Sagiv, J. *Nature* 1988, *332*, 426–429.
(51) Arduengo, A. J.; Moran, J. R.; Rodriguez-Parada, J.; Ward, M. D. *J. Am. Chem. Soc.* 1990, *112*, 6153–6154.

CONCLUSIONS AND PROSPECTUS

A new type of thin film piezoelectric resonator has been described and tested as a mass sensor. The resonator operates at ~1 GHz, exhibiting high mass sensitivities (~−550 cm²/g). The potential application of these resonators as sensors for the detection of gas-phase analytes has also been demonstrated through a primitive manipulation of the sorption selectivity of the structure of the resonator surface. The results of these tests, combined with the small size and potential for low-cost manufacturing, indicate that TFRs may prove valuable in a variety of chemical-sensor applications. It is also important to note that the relatively simple geometric electrode design of TFRs facilitates fabrication relative to the narrow line widths and interdigitated electrode design of SAW and flexural plate devices. Further, since the TFRs are produced on a Si substrate, it is possible to integrate the support electronics required for operation in a single integrated circuit package.[19] Support electronics could include an indicator and a reference TFR, oscillator circuits for both TFRs, and a mixer to produce a difference frequency from the two TFRs. Such a design would minimize temperature and nonspecific adsorption effects through the use of a reference TFR physically close to the indicator TFR. Use of a mixer would also create signals in a lower frequency range, facilitating signal transmission and collection as well as external data processing. Efforts to these ends are in progress. Approaches addressing the fabrication of selective coating materials for industrial process and pollutant monitoring are also underway.

ACKNOWLEDGMENT

M.D.P. gratefully acknowledges the support of a Dow Corning Assistant Professorship. R.P.O. expresses appreciation for a Harpole Graduate Fellowship through the Department of Electrical Engineering at ISU. The fabrication of the TFRs by S. Brayman and D. Schmidt and the assistance of S. Devgun in data acquisition is appreciated. Discussions with H. Shanks and K. Lakin are acknowledged. This work was supported ~~in part~~ by the Center for Advanced Technology Development at Iowa State University under USDOC Grant ITA 87-02 and ~~in part~~ by the Office of Basic Energy Research–Chemical Sciences Division of the U.S. Department of Energy. Ames Laboratory is operated for the U.S. Department of Energy under Contract No. W-7405-eng-82.

RECEIVED for review September 10, 1991. Accepted March 17, 1992.

by the Advanced Life Support Division of the NASA-Ames Research Center (CONTRACT No. NAG2-722),